

AperTO - Archivio Istituzionale Open Access dell'Università di Torino

**Subcellular characterization of NAD<sup>+</sup> biosynthesis in metastatic melanoma by using organelle-specific biosensors**

**This is the author's manuscript**

*Original Citation:*

*Availability:*

This version is available <http://hdl.handle.net/2318/1711580> since 2019-09-10T23:02:57Z

*Published version:*

DOI:10.1089/ars.2019.7799

*Terms of use:*

Open Access

Anyone can freely access the full text of works made available as "Open Access". Works made available under a Creative Commons license can be used according to the terms and conditions of said license. Use of all other works requires consent of the right holder (author or publisher) if not exempted from copyright protection by the applicable law.

(Article begins on next page)

# Antioxidants & Redox Signaling

Antioxidants & Redox Signaling: <http://mc.manuscriptcentral.com/liebert/ARS>

## Subcellular characterization of NAD<sup>+</sup> biosynthesis in metastatic melanoma by using organelle-specific biosensors

Journal:	<i>Antioxidants and Redox Signaling</i>
Manuscript ID	ARS-2019-7799.R2
Manuscript Type:	Original Research Communication
Date Submitted by the Author:	n/a
Complete List of Authors:	Gaudino, Federica ; University of Turin, Medical Science Manfredonia, Ilaria; University of Turin, Medical Sciences Managò, Antonella; University of Turin, Medical Sciences Audrito, Valentina; University of Turin, Medical Sciences Raffaelli, Nadia; Università Politecnica delle Marche Vaisitti, Tiziana; University of Turin, Medical Sciences Deaglio, Silvia; University of Turin, Medical Sciences
Keyword:	Models & Methods, Metabolism, Cancer
Manuscript Keywords (Search Terms):	NAD <sup>+</sup> , biosensor, NAMPT, melanoma
Note: The following files were submitted by the author for peer review, but cannot be converted to PDF. You must view these files (e.g. movies) online.	
GaudinoTimelapse cytosolFig2.avi GaudinoTimelapse NucleusFig2.avi GaudinoTimelapse MitochondrionFig2.avi	

SCHOLARONE™  
Manuscripts

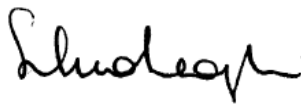
1  
2  
3  
4  
5  
6  
7  
8  
9  
10  
11  
12  
13  
14  
15  
16  
17  
18  
19  
20  
21  
22  
23  
24  
25  
26  
27  
28  
29  
30  
31  
32  
33  
34  
35  
36  
37  
38  
39  
40  
41  
42  
43  
44  
45  
46  
47  
48  
49  
50  
51  
52  
53  
54  
55  
56  
57  
58  
59  
60

Dr Chandan Sen  
Editor in Chief  
*Antioxidants & redox signaling*

Turin, August 9, 2019

**RE: Submission of revision for manuscript ARS-2019-7799.R1 entitled “Subcellular characterization of NAD<sup>+</sup> biosynthesis in metastatic melanoma by using organelle-specific biosensors” by Gaudino and colleagues for publication in your journal as *Original Research Communication*.**

Dear Dr Sen,  
Along with all the authors, I would like to submit the re-revised version for the above-referenced paper. In your email of August 8 to me, you wrote that “additional experimental data are needed”; however, I did not find any indication concerning novel experimental data, which were considered acceptable by all 5 reviewers. In fact, following our first review, we received comments from 5 reviewers, 4 of whom have no further issues at this point and are ok with the revised manuscript. The fifth reviewer suggests further stylistic modifications, most of which are trivial, but does not ask for any additional experimental work. I do not want to sound argumentative, but if you carefully read the modifications required by reviewer 5, you will see that most of them are really within individual writing freedom. However, this reviewer in his/her general comment writes that “the science could be sound”. I find this sentence really unfair: whether the science is sound or not is for the reviewer to decide based upon solid motivations. If the reviewer does not find solid criticism to the science, then he/she should not use derogatory sentences such as the one above. Today, I have carefully gone through all of his/her suggestions and re-wrote the relevant sentences accordingly.  
All modifications are highlighted in red in the revised text.  
Together with all the authors I now hope this work may be rapidly acceptable for publication in *Antioxidants & redox signaling*.



Silvia Deaglio, MD, PhD  
Associate Professor of Medical Genetics  
University of Turin  
Turin, Italy

**REVIEWER 1**

The revised Figure 1 has demonstrated organelle-specific localization for the sensor.

*Author's reply:*

Dear Reviewer 1,

Thanks for acknowledging the organelle specificity of the sensor.

**REVIEWER 2**

The original manuscript has now been improved enough, following reviewers' suggestions.

*Author's reply:*

Dear Reviewer 2,

Thanks for the positive evaluation of our work.

**REVIEWER 3**

The revised manuscript submitted by the authors have satisfactorily addressed the concerns of this reviewer and could be accepted for publication.

*Author's reply:*

Dear Reviewer 3,

Thanks for a positive consideration of our work.

**REVIEWER 4**

No comments

**REVIEWER 5**

This is a revised manuscript. Although the authors have made some effort to address most of my previous comments, there are still serious concerns relating to the readability and comprehension of the manuscript. Too many complex sentences, especially the new additions. In this case, it is challenging to appreciate the merit of the science, which could be sound, but gets murky in convoluted details of awkward sentences.

*Author's reply:*

Dear Reviewer 5,

Thanks for a novel and very thorough stylistic re-review of our paper. As you will see, I have accepted most of your suggestions. However, I am sorry to read that the "science could be sound". I believe that it is your job as a reviewer to judge the soundness of "the science". If you think it is not sound, then you have to say what part of the science is not sound and why. I am also sorry to read that our sentences are "convoluted" and "murky". Again, this should be appropriately detailed. From the examples you make, modifications required are truly minimal, and sometimes arguable. In any case, as you will see from the detailed reply to your issues, I have accepted most of them and explained the reasons why I rejected some. I now hope you will be satisfied, as were the other four reviewers.

**Reviewer's comment:** INTRODUCTION: "First of all, NAD is essential..." Delete "First of all".

*Author's reply:* modified as requested.

**Reviewer's comment:** INTRODUCTION "Open issues concern the biology of the system..." What does this mean?

*Author's reply*

Sentence has been rephrased.

1

2

3 **Reviewer’s comment:** INTRODUCTION “Several efforts were made to elucidate...” Revise to read,

4 “Several efforts have been made to elucidate...”

5 *Author’s reply*

6 As these efforts were well into the past and finished (we refer to published papers!) I am quite sure

7 the past tense is correct. However, to avoid any additional discussion, I modified it as requested.

8

9

10 **Reviewer’s comment:** INTRODUCTION “maintenance of cellular NAD+ pool is pursued through the

11 re-oxidation of...” Change “pursue” to “achieve”.

12 *Author’s reply*

13 Modified as requested.

14

15

16 **Reviewer’s comment:** INTRODUCTION In details...” Revise to read “Briefly...” The scanty information

17 presented is not considered “In details”.

18 *Author’s reply*

19 Modified as requested.

20

21

22

23 **Reviewer’s comment:** INTRODUCTION Last paragraph, line 88 “To the aim, we exploited...” Revise

24 to read, “In addition, we exploited...”

25 *Author’s reply*

26 Here we really mean to say “To the aim”. It does not add to anything else.

27

28

29 **Reviewer’s comment:** RESULTS “Subcellular NAD+ concentrations effects...”

30 Lines 38-40 “Therefore, we hypothesized an NMN-driven rescue of NAD+ levels upon NAMPT

31 chemical inhibition.” What does this mean? Please revise.

32 *Author’s reply.* Sentence was modified as requested

33

34

35 **Reviewer’s comment:** RESULTS FK866 predominantly in nuclei...and in mitochondria...” The

36 statistical significance in comparing the nuclei content seems to be a suspect. Please address.

37 *Author’s reply*

38 This specific experiment was performed 5 independent times. The relevant comparison here is

39 between cells that were treated with FK866 alone and cells that were supplemented with NR before

40 treating with FK866 (as described in Methods).

41 The specific numbers we obtained from the “ratio of ratio” (again details are in Methods) are:

42

FK866	FK866 + NR
1,35	1,26
1,29	1,22
1,2	1,14
1,23	1,13
1,28	1,21

43

44

45

46

47

48

49

50

51

52 Data were statistically analyzed using a paired t test. The results is p=0.0004 and is considered by

53 GraphPad software highly significant.

54

55 **Reviewer’s comment:** RESULTS Lines 48-50 “In the latter, NR preserved NAD+ levels...FK856

56 exposure.” What does this sentence mean? Consider simplifying it. Similar concern in clarity is

57 applicable to the sentence, lines 52-60 “Treatment of A375 with QA...increased NAD levels only in

58 mitochondria. Furthermore, selectively in these organelles...FK866-induced NAD depletion...”

59 Please revise the two sentences cited here.

60

*Author's reply*

Sentences were modified to improve readability.

**Reviewer's comment:** RESULTS Proof-of-principle of the...  
Line 45 "The result is in keeping with literature suggesting..." Revise to read, "The result is consistent with the literature, suggesting..." Line 50-52 "...with our data indicating that NAMPT is mostly cytosolic enzyme..." This phrase seems as redundant and therefore, not necessary.

*Author's reply*

Modified as indicated

**Reviewer's comment:** DISCUSSION Lines 33-37 "Even if promising, initial trials have limited clinical responses, also because they were burdened by significant.... Please revise for clarity of meaning.

*Author's reply*

Thanks for pointing this out, sentence was rephrased.

**Reviewer's comment:** DISCUSSION Paragraph starting with "Characterization of subcellular NAD pool...", line 59 "...support increased cellular growth rates they reprogram NDA+ biosynthesis. Replace "reprogram" with "reprogrammed".

*Author's reply*

Modified

**Reviewer's comment:** DISCUSSION Lines 28-30 "Indeed, for these cells, HPLC measurements already detected more than the double of NAD+ content..." Revise to read, "Indeed, for these cells, HPLC measurements detected more than double the NAD+ content..."

*Author's reply*

Modified

**Reviewer's comment:** DISCUSSION Lines 15-23 "The current view of the field is that NRKs are preferentially located in cytosol...no evidence is available indicating NRK activity in this organelle." Revise to read, "The current view of the field is that NRKs are preferentially located in the cytosol...no evidence is available for NRK activity in mitochondria.

*Author's reply*

Modified

**Reviewer's comment:** DISCUSSION Lines 47-52 "Our data, both biochemical and biosensor based...arguing in favor of direct NAD biosynthesis in these organelles." Revise to read "Our data, both biochemical and biosensor based...arguing in favor of direct NAD biosynthesis in the organelle."

*Author's reply*

I did not modify this, but kept the original version. Mitochondria is plural, the organelle is singular, so I prefer these organelles.

1  
2  
3  
4  
5  
6  
7  
8  
9  
10  
11  
12  
13  
14  
15  
16  
17  
18  
19  
20  
21  
22  
23  
24  
25  
26  
27  
28  
29  
30  
31  
32  
33  
34  
35  
36  
37  
38  
39  
40  
41  
42  
43  
44  
45  
46  
47  
48  
49  
50  
51  
52  
53  
54  
55  
56  
57  
58  
59  
60

**Reviewer’s comment:** DISCUSSION Lines 54-6, starting with Chowdhry et al....” to “NRK knockdown or dual inhibition...” on the next page (all in red) should be revised for the sake of clarity; the paragraph does not make sense.

*Author’s reply*

Sentence re-written

**Reviewer’s comment:** DISCUSSION Lines 18-20 “...however, we cannot exclude the cytosolic import of NAD, a possible enzyme translocation mechanism or cell type dependence of NAD+...” This phrase is difficult to understand in context.

*Author’s reply*

Sentence re-written

**Reviewer’s comment:** DISCUSSION Lines 25-33 “At the concentrations used...regulated transport of these metabolites.” This is a long and tortuous sentence. Please fragment it to two easy to understand sentences.

*Author’s reply*

Sentence re-written

**Reviewer’s comment:** DISCUSSION Line 40 “...compartment the NR >>NAD+ pathway is NAMPT-dependent rather than NRK-dependent.” What does this phrase men? Please clarify.

*Author’s reply*

This refers to data contained in references 5 and 36. It has been rephrased to improve clarity.

**Reviewer’s comment:** DISCUSSION Line 49 “Overall, our data provide proof-of-principle...to monitor NAD+ fluctuations occurring in...” Revise to read, “Overall, our data provide proof-of-principle...to monitor NAD+ fluctuations that occur in...”

*Author’s reply*

Modified

Gaudino F., et al.

## Original Research communication

**Title:** Subcellular characterization of NAD<sup>+</sup> biosynthesis in metastatic melanoma by using organelle-specific biosensors

**Authors:** Federica Gaudino<sup>1</sup>, Ilaria Manfredonia<sup>1</sup>, Antonella Managò<sup>1</sup>, Valentina Audrito<sup>1</sup>, Nadia Raffaelli<sup>2</sup>, Tiziana Vaisitti<sup>1</sup>, Silvia Deaglio<sup>1</sup>.

**Affiliations:** <sup>1</sup>Department of Medical Sciences, University of Turin, Turin, 10126 Italy; <sup>3</sup>Department of Clinical Sciences and Department of Agricultural, Food and Environmental Sciences, Polytechnic University of Marche, Ancona, 60121 Italy.

**Running head:** Subcellular NAD<sup>+</sup> biosynthesis in melanoma

**Corresponding author:** Silvia Deaglio, MD, PhD, Department of Medical Sciences, University of Turin, via Nizza, 52, 10126 Torino, Italy. Phone: (+39-011) 670-9535. Email: [silvia.deaglio@unito.it](mailto:silvia.deaglio@unito.it).

**Keywords:** NAD<sup>+</sup>, BIOSENSOR, NAMPT, MELANOMA, METABOLISM.

**Word count:** 4335

**Number of references:** 65

**Number of color figures:** 4

**Number of black and white figures:** 4

**Acknowledgements:** This work was supported by the GILEAD Fellowship Program (Gilead Italia 2018 to SD) and by the Ministry of Education, University and Research, PRIN Project 2017CBNCT (to SD) and “Dipartimenti di Eccellenza 2018–2022” (project #D1518000410001) to the Department of Medical Sciences of the University of Turin.



Gaudino F., et al.

**Abstract**

**Aim:** NAD<sup>+</sup> plays central roles in a wide array of normal and pathological conditions. Inhibition of NAD<sup>+</sup> biosynthesis can be exploited therapeutically in cancer, including melanoma. To obtain quantitation of NAD<sup>+</sup> levels in live cells and to address the issue of the compartmentalization of NAD<sup>+</sup> biosynthesis, we exploited a recently described, genetically-encoded NAD<sup>+</sup> biosensor (LigA-cpVENUS), which was targeted to the cytosol, mitochondria and nuclei of BRAF-V600E A375 melanoma cells, a model of metastatic melanoma (MM).

**Results:** FK866, a specific inhibitor of nicotinamide phosphoribosyltransferase (NAMPT), the main NAD<sup>+</sup>-producing enzyme in MM cells, was used to monitor NAD<sup>+</sup> depletion kinetics at the subcellular level in biosensor-transduced A375 cells. In addition, we treated FK866-blocked A375 cells with NAD<sup>+</sup> precursors, including nicotinamide, nicotinic acid, nicotinamide riboside and quinolinic acid, highlighting an organelle-specific capacity of each substrate to rescue from NAMPT block. Expression of NAD<sup>+</sup> biosynthetic enzymes was then biochemically studied in isolated organelles, revealing presence of NAMPT in all three cellular compartments, while NAPRT was predominantly cytosolic and mitochondrial, and NRK mitochondrial and nuclear. In keeping with biosensor data, QPRT was expressed at extremely low levels.

**Innovation & Conclusions:** Throughout this work, we validated the use of genetically encoded NAD<sup>+</sup> biosensors to characterize subcellular distribution of NAD<sup>+</sup> production routes in MM. The chance of real time monitoring of NAD<sup>+</sup> fluctuations after chemical perturbations, together with a deeper comprehension of the cofactor biosynthesis compartmentalization, strengthens the foundation for a targeted strategy of NAD<sup>+</sup> pool manipulation in cancer and metabolic diseases.

Gaudino F., et al.

## Introduction

Nicotinamide adenine dinucleotide (NAD<sup>+</sup>) is a vital, ubiquitous and multifunctional cofactor regulating a wide range of biological processes (10,29). NAD<sup>+</sup> is essential as electron acceptor donor in glycolytic, tricarboxylic acid cycle (TCA) and oxidative phosphorylation redox reactions. The equilibrium existing between its oxidized (NAD<sup>+</sup>) or reduced forms (NADH) mediates cellular antioxidation mechanisms, as well as cell redox state homeostasis, energy metabolism and mitochondrial functions (62). In addition, NAD<sup>+</sup> is the substrate of enzymes with fundamental roles in gene expression and cell signaling, independent of its redox properties. This large family of NAD<sup>+</sup> consuming enzymes includes adenosine diphosphate (ADP)-ribose transferases (ARTs) and poly ADP-ribose polymerases (PARPs), sirtuins (SIRTs) and cyclic ADP-ribose hydrolases (CD38/CD157) (27,57). Through their functional activities of post-translational modifications (ADP-ribosylation and deacetylation reactions), or by calcium signaling mobilization, these enzymes regulate gene transcription, cell differentiation, cell cycle progression, DNA repair, chromatin stability, among other biological processes (12), representing connecting elements between the metabolic state of a cell and its signaling and transcriptional activities.

The subcellular localization of specific biosynthetic pathways remains to be fully elucidated. Several efforts have been made to elucidate where NAD<sup>+</sup> biosynthesis occurs and whether there are exchanges between compartments (17,18,30,31,40,46). The maintenance of cellular NAD<sup>+</sup> pool is achieved through the re-oxidation from NADH or through the active synthesis of the pyridine nucleotide. Briefly, NAD<sup>+</sup> is synthesized through one *de novo* bio-synthetic pathway, starting from tryptophan/quinolinic acid (QA) and controlled by the enzyme quinolinate phosphoribosyltransferase (QPRT) (6,29) and three salvage pathways involving nicotinamide (NAM), nicotinic acid (NA), and nicotinamide riboside (NR) (12,34). Each pathway is controlled by a rate-limiting enzyme, specifically nicotinamide phosphoribosyl transferase (NAMPT), nicotinate

*Gaudino F., et al.*

phosphoribosyltransferase (NAPRT) and nicotinamide riboside kinase (NRK). Among these pathways, the reaction controlled by NAMPT is the most relevant in mammalian cells (48), as the NAMPT substrate, NAM, is released by the main NAD<sup>+</sup> consuming enzymes, such as sirtuins and PARPs, connecting NAD<sup>+</sup> synthesis and degradation in a functional loop. NAMPT is frequently over-expressed in hematological and solid tumors (22,35,52). Our recent data showed that transformation of melanocytes to metastatic melanoma (MM) is accompanied by a net increase in global NAD<sup>+</sup> levels, particularly in the BRAF-mutated subset (2). Further elevation of NAD<sup>+</sup> levels occurs in cells that acquire resistance to BRAF inhibitors, an event accompanied by metabolic reprogramming and NAMPT overexpression (2,3). An increase in NAD<sup>+</sup> may be needed to sustain cell proliferation and growth of MM cells and it may directly affect NAD<sup>+</sup> consumption pathways in an organelle-specific manner.

Following this hypothesis, we studied NAD<sup>+</sup> bioavailability by dissecting the subcellular location of its biosynthesis. To the aim, we exploited a genetically-encoded fluorescent biosensor (9,15,19) to directly monitor free NAD<sup>+</sup> concentrations in subcellular compartments of MM cells and we connected this information to the biochemical evaluation of subcellular distribution of NAD<sup>+</sup> biosynthetic enzymes (NBEs).

**Results**

**Generation of A375 cells stably expressing organelle-specific NAD<sup>+</sup> biosensor**

Gaudino F., et al.

To study the compartmentalization of NAD<sup>+</sup> biosynthesis, we used the BRAFV600E-mutated A375 cell line as a melanoma model. Both, BRAF inhibitor sensitive (S) and resistant (BiR) A375 were transduced with lentiviruses carrying the DNA coding for organelle-specific biosensor proteins (9). The biosensor contains an organelle specific sequence (as detailed in M&M), and the NAD<sup>+</sup>-binding site of a bacterial DNA ligase (LigA1b-LigA1a). A cpVENUS fluorescent protein is connected to the bipartite NAD<sup>+</sup> binding domain of the enzyme. The structure allows biosensor fluorescence to be turned off when NAD<sup>+</sup> is bound. Based on their cpVENUS-fluorescence, transduced cells were flow-sorted to obtain stably expressing cells. Confocal microscopy shows the specificity of the biosensor in reaching the target compartment (Figure 1 A-B-C), as determined by co-localization of the biosensor signal (green) with the actin cytoskeleton (red), TOM20 (magenta) or DAPI (blue).

#### **Organelle-specific effects of NAMPT inhibition**

To study NAD<sup>+</sup>-depletion kinetics induced by inhibiting the major mammalian NAD<sup>+</sup> biosynthetic pathway, we treated biosensor-encoding A375 cells with the well-known NAMPT inhibitor FK866 (2,38). The biosensor works by decreasing its fluorescence at 488 nm in the presence of increased levels of NAD<sup>+</sup>, while its 405 nm fluorescence is unaffected by substrate variations and can be used to normalize the biosensor expression levels. Therefore, a decrease in NAD<sup>+</sup> levels leads to an increase of the 488 nm/405 nm fluorescence ratio (9,15,19). From previous works, it is known that FK866 treatment leads to a significant drop of total intracellular NAD<sup>+</sup> levels beginning few hours after treatment (26). Consistently, a time-lapse confocal microscopy analysis of A375 cells treated with FK866 (25nM), confirmed a net drop in cytosolic, mitochondrial and nuclear NAD<sup>+</sup> levels steadily increasing over the 4 hours observation time (Figure 2A, movies 1-2-3). In order to obtain quantitative measurements, we then measured NAD<sup>+</sup> concentrations by cytofluorimetric analysis, at the fixed time point of 16 hours after FK866 treatment, when >90% of intracellular NAD<sup>+</sup> is depleted, according to previous data (9). In these conditions, we observed a sharp increase in the

Gaudino F., et al.

488 nm/405 nm fluorescence ratio in FK886-treated cells in all the sub-cellular compartments (Figure 2B). The mean fluorescence ratio was augmented by  $30\pm10\%$  ( $p=0.0002$ ),  $38\pm14\%$  ( $p<0.0001$ ) and  $32\pm9\%$  ( $p<0.0001$ ) in the cytosol, mitochondria and nuclei, respectively. Figure 2C is a representative example of the biosensor behavior under FK866 treatment. The dot plot on the left depicts changes in fluorescence at 488 nm in relation to 405 nm of cell expressing the biosensor or the cpVENUS only. No modification in the 488 nm fluorescence of the cpVENUS could be highlighted after treatment with FK866, confirming specificity of the results (relative histograms on the right).

**Subcellular NAD<sup>+</sup> concentrations and effects of NMN on subcellular NAD<sup>+</sup> levels**

In order to quantify NAD<sup>+</sup> fluctuations, we generated specific calibration curves for the cytosolic, the nuclear and the mitochondrial biosensors (Figure 3) (9,15,19). To do so, cells expressing cytosolic and nuclear biosensors were saponin-permeabilized to allow exogenous NAD<sup>+</sup> (used in a range of concentrations between 0 and 4 mM for cytosol and from 0 to 3mM for nucleus) to enter the cell or nucleus, as previously described (9). For the mitochondrial biosensor, saponin permeabilization was followed by rapid treatment with the ion channel-forming peptide alamethicin (AlaM), which renders mitochondria permeable to low-molecular-mass molecules (4,23,37). In this conditions, exogenous NAD<sup>+</sup> (from 0 to 10mM) entered in the organelle, inducing a linear reduction of the sensor fluorescence according to increasing NAD<sup>+</sup> concentrations. Table 1 shows fluorescence ratio 488 nm/405 nm calculations obtained from each biosensor and normalized on relative cpVENUS 488 nm/405 nm variations (for cytosolic and nuclear biosensors the mean of 4 replicates is shown, while 3 replicates are shown for mitochondrial biosensor). These cytofluorimetric measurements of fluorescence variations at each NAD<sup>+</sup> concentration were used to build specific sigmoidal curves. Lastly, by interpolating fluorescence ratio of non-permeabilized cells expressing the cytosolic biosensor to the relative titration curve, we found basal cytosolic mean values of NAD<sup>+</sup> in A375 cells of  $261\pm74\mu\text{M}$ . The same experimental approach was used for the cells expressing the

Gaudino F., et al.

nuclear biosensor, detecting in this compartment a basal nuclear concentration of  $259 \pm 85 \mu\text{M}$ , while  $\text{NAD}^+$  concentrations in the mitochondria were in the range of  $499 \pm 154 \mu\text{M}$ . Treatment with FK866 diminished cytosolic, nuclear and mitochondrial  $\text{NAD}^+$  concentrations to values  $< 0.7 \mu\text{M}$ , below which the system is no longer sensitive. The amount of this  $\text{NAD}^+$  depletion is in line with previously reported HPLC measurements of whole lysates from FK866-treated A375 cells (2).

Next, to further validate the system in our model, we studied the effects of nicotinamide mononucleotide (NMN), the product of the reaction catalyzed by NAMPT, on  $\text{NAD}^+$  levels with or without treatment with FK866. After being produced by NAMPT, NMN is converted into  $\text{NAD}^+$  by nicotinamide mononucleotide adenylyl-transferases (NMNATs), which are known to be expressed in the nucleus (NMNAT1), in the cytosol and Golgi (NMNAT-2) and in the mitochondria (NMNAT-3)(7,45,46). Therefore, we hypothesized that supplementation of NMN to cells could rescue  $\text{NAD}^+$  levels in the presence of NAMPT inhibitors. As expected, treatment of A375 cells with NMN increased basal  $\text{NAD}^+$  levels, in all cellular compartments and particularly in the cytosol (Figure 3C). After treating cells with the NMNAT substrate, we detected a consistent reduction of fluorescence ratio of  $14 \pm 2\%$  ( $p=0.001$ ) in the cytosol corresponding to an increase in  $\text{NAD}^+$  to  $1621 \pm 606 \mu\text{M}$ . In the nuclei, a reduction of fluorescence in the range of  $8 \pm 4\%$  ( $p=0.0037$ ) corresponded to  $651 \pm 280 \mu\text{M}$   $\text{NAD}^+$ . A moderate but consistent fluorescence reduction of  $9 \pm 3\%$  ( $p=0.043$ ) was also detected in mitochondria, where we measured an increase of the cofactor to a mean value of  $2012 \pm 1855 \mu\text{M}$ . Importantly, the combination of NMN and FK866, reverted the FK866-induced fluorescence ratio from  $36 \pm 5\%$  to  $6 \pm 7\%$  ( $p=0.01$ ) in the cytosol, from  $35 \pm 13\%$  to  $8 \pm 6\%$  ( $p=0.002$ ) in the mitochondria and from  $28 \pm 7\%$  to  $16 \pm 8\%$  ( $p=0.021$ ) in the nuclei. The NMN-dependent rescue of NAMPT block is statistically significant when considering fluorescence ratios, and  $\text{NAD}^+$  levels recover from  $< 0.7 \mu\text{M}$  to  $167 \mu\text{M}$  in cytosol, to  $125 \mu\text{M}$  in mitochondria and to  $9 \mu\text{M}$  into the nucleus.

#### Topography of $\text{NAD}^+$ Biosynthesis: NAM and NA primarily affect cytosolic $\text{NAD}^+$ levels

*Gaudino F., et al.*

To obtain a complete topography of NAD<sup>+</sup> biosynthesis in MM, we then studied the efficacy of different NAD<sup>+</sup> precursors including NAM, NA, NR and QA, in sustaining NAD<sup>+</sup> biosynthesis and in rescuing from FK866-mediated NAD<sup>+</sup> depletion in the various compartments. We first treated cells with NAM and NA, substrates of the most relevant NAD<sup>+</sup> producing pathways in MM cells. NAM is recycled to NAD<sup>+</sup> in a two-step salvage pathway in which NAMPT, using the ribose-5-phosphate group of phosphoribosylpyrophosphate (PRPP) catalyzes a phosphoribosyl transferase reaction converting NAM to NMN (31). Treatment of cells with NAM led to a significant increase in cytosolic NAD<sup>+</sup> basal levels, as expected based on the documented cytosolic expression of NAMPT (2,17,40) (Figure 4A). In fact, in this compartment, the fluorescence ratio was reduced by 17±7% (p=0.004), corresponding to an increase in basal NAD<sup>+</sup> levels to 1930±980μM. A slighter decrease in the fluorescence ratio was observed in the nuclei, where we measured an increase in basal levels of the cofactor to 489±195μM, whereas no changes were measured in mitochondria. An additional mechanism leading to NAD<sup>+</sup> accumulation could be linked to block of NAD<sup>+</sup> intracellular consumption, as NAM is a powerful noncompetitive inhibitor of NAD<sup>+</sup>-consuming enzymes (SIRTs and PARPs) (8,31,51). Consistently, even when added to A375 cells treated with FK866, NAM was able to partially prevent NAD<sup>+</sup> loss. In fact, in the cytosol, we observed a rescue from FK866-induced NAD<sup>+</sup> depletion, with fluorescence ratios going from 29±14% to 15±13% (p=0.02, NAD<sup>+</sup> concentration of 36μM), in mitochondria from 46±20% to 14±20% (p=0.005), while in the nuclear compartment from 37±6% to 23±8% (p=0.003). The observed NAM-driven rescue of NAD<sup>+</sup> levels, would essentially reflect the inhibition of sirtuin activities in the three compartments, while in the nuclei PARPs activity block could also contribute to the outcome.

NA is the substrate of NAPRT, which converts NA into nicotinic acid mononucleotide (NAMN) via the Press-Handler pathway (11,29). NA was effective in the cytosol, as well in nuclei and mitochondria, both in increasing compartmentalized NAD<sup>+</sup> basal levels and in countering the effects of NAMPT



Gaudino F., et al.

inhibition (Figure 4B). The highest NA-dependent increase in basal NAD<sup>+</sup> was detected in the cytosol (13±4% of fluorescence ratio reduction, p=0.013, NAD<sup>+</sup> concentration of 976±550μM), followed by mitochondria (1031±550μM). The evidence of a NA/NAPRT-mediated rescue from FK866-induced NAD<sup>+</sup> depletion, confirms the reported finding that NAPRT-mediated NAD<sup>+</sup> production limits the action of NAMPT inhibitors used in cancer treatment (42,53).

### **Topography of NAD<sup>+</sup> Biosynthesis: NR and QA showed an organelle-specific impact on NAD<sup>+</sup> levels**

We then tested the effects of NR and QA on subcellular NAD<sup>+</sup> levels. NR is an additional salvageable NAD<sup>+</sup> precursor via the NRKs-mediated pathway. NR conversion to NAD<sup>+</sup> is initiated by phosphorylation of NR to NMN by NR kinases (NRKs) (47,56). Studying the subcellular capacity of NR in sustaining NAD<sup>+</sup> production in MM, we found NR to be effective in increasing basal NAD<sup>+</sup> levels in cytosol (760±557μM) and in nuclei (533±166μM) (Figure 5A). However, NR was able to counter the effects of FK866 predominantly in nuclei (from 27±5% to 19±5% p=0.0004) and in mitochondria (from 37±12% to 14±11% p=0.007) (Figure 5A). In mitochondria of cells supplemented with NR and treated with FK866, NAD<sup>+</sup> levels were kept between 50-240μM, thus preventing its drop after FK866 exposure. Lastly, treatment of A375 with QA, an intermediate precursor of the 8 steps-*de novo* synthesis pathway, increased NAD<sup>+</sup> levels only in mitochondria. Furthermore, QA offered partial and weak protection from FK866-induced NAD<sup>+</sup> depletion selectively in mitochondria (Figure 5B). This finding is in line with the reported low expression of QPRT in MM (2,29). Together, these results support the idea of a dominant NAD<sup>+</sup> production via the recycling pathways in MM cells, with a clear preference for the cytosolic NAM-NAMPT. In the cytosol NAPRT can be considered a second active NAD<sup>+</sup> producer, while in the organelles, NRK appears to play a key role as NAD<sup>+</sup> biosynthetic enzyme.

### **Subcellular localization of NAD<sup>+</sup> biosynthetic enzymes**

Subcellular distribution of NBEs remains an incompletely understood aspect of NAD<sup>+</sup> physiology, with increasing evidence suggesting that NAD<sup>+</sup> biosynthesis is compartmentalized in a cellular- and



*Gaudino F., et al.*

tissue-dependent way (17,46). To determine the subcellular expression pattern of NBEs in A375 cells in exponential growth phase and to interpret data obtained with the organelle-specific biosensors, we used confocal microscopy and biochemical analyses. Western blot analyses were performed on cytosol and isolated mitochondria and nuclei. Confocal microscopy was used to support biochemical analysis. By comparing expression levels of the four NBEs, we confirmed that NAMPT is the dominant NBEs (Figure 6A-C, left panel). We then dissected NBEs subcellular localization by looking at protein distribution in the separate compartments. A percentage of expression for the different compartments was determined by dividing pixel intensity of the specific bands pertaining to a given compartment by the sum of the pixel intensities of the bands pertaining to all compartments. Western blot analysis showed that NAMPT is mostly cytosolic (84.16% of localization, Figure 6A), with low mitochondrial (10.74%) and nuclear (5.1%) expression. Organelles purity was confirmed by using specific markers (anti-Vinculin, -tubulin,-actin antibodies specifically highlight cytosolic fraction; anti-hadha and -cytochrome C antibodies identify mitochondrial enrichment while anti-H2A antibody was used for nuclear compartment detection). NAPRT was essentially cytosolic (92.2%), with minor fractions present in mitochondria (5.7%) and nuclei (2.1%). Conversely, NRK was mostly mitochondrial (67.2%) and nuclear (32.7%). QPRT was detectable at very low levels only in cytosol and in mitochondria (not shown). Organelle purity was confirmed by using specific markers. NBEs subcellular distribution was confirmed by confocal microscopy, by using organelle-specific markers and a software co-localization tool (Figure 6C, right panel). The panel on the left shows the overlay of the NBE under analysis and the compartment specific marker. The three panels on the right show expression of the NBE under analysis in the indicated compartment.

**Proof-of-principle of the use of the biosensor to monitor NAD<sup>+</sup> levels**

Lastly, we decided to use the biosensor to compare NAD<sup>+</sup> levels in A375 cells before (S) and after the acquisition of resistance to BRAF inhibitors (BiR). These cellular models offered us a strategic

Gaudino F., et al.

and clinically relevant example of cancer metabolic adaptation suitable for characterization of NAD<sup>+</sup> biosynthesis. In keeping with our prior data showing that A375/BiR cells are characterized by higher expression of NAMPT and constitutive higher levels of NAD<sup>+</sup> (2), the biosensors showed a more pronounced sensitivity to NAD<sup>+</sup>-depletion through NAMPT inhibition. Specifically, as evidenced by a higher fluorescence variations, upon FK866 treatment, A375/BiR cells were more severely NAD<sup>+</sup>-depleted than /S variants, at least in the cytosol and nucleus (Figure 7). These results, not only confirm that NAMPT is the master regulator of NAD<sup>+</sup> biosynthesis in A375/BiR cells, but also evidence a compartmentalized response to NAMPT inhibition in the two cell lines. Specifically, a highly significant difference in response to FK866 was highlighted in the cytosol and the nuclei, while no significant difference was observed in mitochondria. This result is consistent with the literature suggesting a differential behavior of mitochondria compared to the cytosol or the nuclei in the dynamics of metabolites exchange (40,53). In addition, we found that, in A375, the most mitochondrial expressed NBE is NRK, potentially explaining the lower sensitivity of A375/BiR mitochondria to NAMPT inhibition.

Overall, these data validate NAD<sup>+</sup> biosensors as tools to understand whether the main pathways responsible for NAD<sup>+</sup> production differ across subcellular compartments or under chemical perturbations.

Gaudino F., et al.

**Discussion**

Because of its essential role and ubiquitous presence, alterations of NAD<sup>+</sup> concentrations are associated with a large number of pathological conditions, including metabolic diseases like obesity, diabetes and insulin resistance, inflammation and immune responses (16,46,64). A decrease in NAD<sup>+</sup> levels is also a hallmark of aging and aging-associated pathologies, such as neurodegeneration and motor function decline. For these reasons, NAD<sup>+</sup> boosting molecules or inhibitors of the NADases received remarkable attention as antiaging agents or co-adjuvants for maintaining NAD<sup>+</sup> homeostasis (46). On the other hand, a significant branch of research on NAD<sup>+</sup> metabolism documented increased levels of the cofactor during tumorigenesis (2,52), thus rendering NAD<sup>+</sup> metabolism an attractive therapeutic target in cancer treatment. Inhibitors against NAMPT, the major intracellular NBE, are under development for phase I and II clinical trials for patients with ovarian, pancreatic and rectal cancers or with hematological malignancies, including multiple myeloma and chronic lymphocytic leukemia (28,58,60). Even if some clinical responses were observed, patients treated with NAMPT inhibitors experienced significant toxicity, including thrombocytopenia and gastrointestinal complications. The modest success of FK866 in cancer patients, may be explained by the activation of rescue pathways that can overcome NAMPT block and restore NAD<sup>+</sup> levels through alternative routes. Most important in this context is NAPRT, the rate-limiting enzyme in the metabolism of dietary NA into NAD<sup>+</sup>. Epigenetic regulation of NAPRT leads to gene silencing in some tumors, while in the cases in which it is over-expressed, the enzyme is responsible for the failure of NAMPTi-based treatments (11,42). Like NA, NR can be introduced through diet, but it is also the by-product of extracellular NMN dephosphorylation reaction carried out by CD73 (53), an ectoenzyme involved in the generation of adenosine, in turn a powerful immunosuppressant. Recent reports indicate that NR, via NRK activity, maintains cancer NAD<sup>+</sup> homeostasis in the presence of NAMPTi, contributing to treatment failure (14,25,53). In addition,

Gaudino F., et al.

the dynamic  $\text{NAD}^+/\text{NADH}$  balance impacts on the redox state of cancer cells. In fact, tumors possess higher levels of reactive oxygen species (ROS), rendering them more sensitive to changes in the redox status (13,33). In this context,  $\text{NAD(H)}/\text{NADP(H)}$  balance regulates glutathione reductase (GR) and thioredoxin reductase (TR) activities, major components of the antioxidant defense system (24,39,59). Specifically, reducing equivalents from NADPH are used to regenerate reduced glutathione (GSH) from the oxidized form (GSSG), fueling the ROS scavenging system of the cell (59). For this reason, the availability of  $\text{NAD}^+$  precursors and their subcellular-specific employment could regulate the activity of GSH/GSSG system in an organelle-dependent way. The prevalence of a cytosolic GSH pool likely makes it sensitive to the presence of an active NAM/NAMPT axis and to its pharmacological inhibition. In addition, G6PD, which is the major source of NADPH, can also be activated post-transcriptionally by SIRT2 dependent deacetylation (59).

Characterization of subcellular  $\text{NAD}^+$  pools and compartmentalized  $\text{NAD}^+$  biosynthetic pathways are pivotal in order to tailor therapeutic interventions, modulating the balance between  $\text{NAD}^+$  consumption and production. This work was undertaken with the dual aim of obtaining a clearer picture of  $\text{NAD}^+$  biosynthesis in BRAF-mutated melanoma cells and to set-up conditions to follow its modifications in live cells. To address our aims, out of all the tools developed in the last 10 years for real time measuring of  $\text{NAD}^+$  or  $\text{NAD}^+/\text{NADH}$  levels (50,65), we used a recently devised genetically-encoded  $\text{NAD}^+$  biosensor (9), which was targeted to the cytosol, nuclei and mitochondria. The choice of this biosensor is based on its intrinsic properties I) as a ratiometric tool specific for  $\text{NAD}^+$  detection, II) optimal binding affinity for physiological cellular  $\text{NAD}^+$  concentrations. In addition, III) the biosensor is easy to manipulate and has equally easy readouts.

BRAF-V600E A375 cells were used as experimental model, as it was shown that, in order to support increased cellular growth rates, they **reprogrammed**  $\text{NAD}^+$  biosynthesis by overexpressing NAMPT. This NAMPT overexpression is even stronger during BRAF inhibitors resistance development (2,3), a

*Gaudino F., et al.*

frequent clinical complication incurring in metastatic melanoma of patients. The basal NAD<sup>+</sup> concentration in the cytosol and nuclei of A375 cells in the exponential growth phase was estimated at 260μM and at 499μM in mitochondria (Figure 8), in keeping with previously reported values for total intracellular free NAD<sup>+</sup> levels ranging between 200 and 500μM (10,29,31,57,61). In addition, in basal conditions, the recently estimated NAD<sup>+</sup> pool concentrations in cultured mammals and murine derived cell lines (HEK293T, HeLa, U2OS, NIH3T3) move from 60μM to 120μM for nuclei and cytosol (9,29,50), increasing to ~300μM in mitochondria (9,10,29). These reported compartmentalized NAD<sup>+</sup> concentrations are tightly dependent on the cell type. For this reason, it was not surprising for us to find the aforementioned concentration of free NAD<sup>+</sup> in cytosol, nuclei and mitochondria of A375 cells. Indeed, for these cells, HPLC measurements already detected more than double the NAD<sup>+</sup> content compared to normal melanocytes (2). Moreover, by combining dynamic measurements using live cells and organelle fractionation, we can conclude that NAMPT is quantitatively the most expressed NAD biosynthetic enzyme in A375 cells and undoubtedly the dominant one in the cytosol (Figure 8). If we look at the nuclear compartment, the prevalent NBE is NRK followed by NAMPT. Cytosol and nuclei are considered exchangeable compartments for the diffusion of NAD<sup>+</sup> pools (31). This concept, together with the revealed high expression levels of NRK in nuclei, could explain similar levels of NAD<sup>+</sup> concentrations between cytosol and nucleus of A375. By combining two well established protocols for mitochondria purification (21,32,63), we found that mitochondria of MM cells appear to be equipped predominantly with NRK and possibly with lower levels of NAMPT and NAPRT (Figure 8). Even though mitochondrial NAD<sup>+</sup> contents can reach up to 70% of total intracellular NAD<sup>+</sup> (1), how its levels are maintained remains a matter of debate. Two processes, glycolysis and NAD<sup>+</sup> biosynthesis, directly link cytoplasmic and mitochondrial NAD<sup>+</sup> pools (54). The NADH produced by glycolysis is transported into the mitochondrial matrix by NAD<sup>+</sup>/NADH redox shuttles (62), providing reducing equivalents for the TCA cycle and electron transport chain

Gaudino F., et al.

(ETC). The former process reduces  $O_2$  to water and NADH to  $NAD^+$  in order to produce ATP, generating mitochondrial  $NAD^+$  levels much higher than the other cellular compartment (43). In addition, maintenance of  $NAD^+$  levels in the compartment is also dependent on salvaging NAM produced by  $NAD^+$ -consuming enzymes. The current view of the field is that NRKs are preferentially located in the cytosol and nucleoplasm, and while it is accepted that NR is the preferred  $NAD^+$  precursor for mitochondrial  $NAD^+$  synthesis (29,40,53), no evidence is available indicating NRK activity in mitochondria. One of the current hypotheses about mitochondrial  $NAD^+$  is that, it can be maintained by the NMNAT3 conversion of NMN or by the membrane transport of  $NAD^+$  precursors (NAM, NMN) or even  $NAD^+$  itself. Indeed, while some demonstrated that  $NAD^+$  is unable to cross the mitochondrial membrane and that pyridine nucleotides are instead broken down to the corresponding nucleosides (40,44,53,54), others affirmed that only intact  $NAD^+$  can restore depleted mitochondria  $NAD^+$  levels (17,20). Even if the first eukaryotic mitochondrial  $NAD^+$  carrier, named Ndt1p, was identified in *Saccharomyces cerevisiae* (55) and in 2009 Palmieri et al. identified a chloroplast and mitochondrial  $NAD^+$  carrier protein in *Arabidopsis thaliana* (41), no mammalian transporter for  $NAD^+$  has yet been found. For these reasons, whether there is a complete  $NAD^+$  biosynthetic apparatus or a system transport for  $NAD^+$  in mitochondria remains unclear (17). Our data, both biochemical and biosensor based, suggest that NRK is present in the mitochondria, at least in A375 melanoma cells, arguing in favor of direct  $NAD^+$  biosynthesis in these organelles. In addition, the prevalent NRK expression in mitochondria, could suggest the use of NRK inhibitors. Consistently, recent data by Chowdhry et al. indicated that NRK-dependent synthesis of  $NAD^+$  causes the failure of NAMPTi and that both NRK knockdown or dual inhibition of NAMPT and NRK lowered the dose of FK866 needed to arrest tumour growth, leading to persistent tumor regression *in vivo* (14).

Gaudino F., et al.

Intracellular NAMPT is ubiquitously present in human body, even if its expression varies according to tissues (46,49). Different experimental approaches have been exploited to define mitochondrial presence of NAMPT in different cell lines with controversial results (9,17,29,40,61). We found that also mitochondria are sensitive to NAMPT inhibition and that a small amount of NAMPT is present in these organelles. However, alternative explanations, such as cytosolic import of NAD<sup>+</sup> cannot be excluded, as well as a cell type dependence of NAD<sup>+</sup> biosynthetic pathways localization. At the concentrations used, NA raised NAD<sup>+</sup> levels rescued FK866-dependent NAD<sup>+</sup> depletion in all compartments, pointing to a very efficient NAPRT pathway. On the contrary, neither NR nor NAM raised NAD<sup>+</sup> levels in mitochondria even though both NRK and NAMPT are present in the organelles. The finding that NMN induced a slight increase of mitochondrial NAD<sup>+</sup> may reflect regulated transport of these metabolites. With the exception of QA, all tested NAD<sup>+</sup> precursors, including NMN, are effective in boosting NAD<sup>+</sup> levels in cytosol and nuclei. Among them, only NR is unable to rescue the FK866-induced NAD<sup>+</sup> depletion in cytosol, in keeping with previous data that suggest that the NAM and NR pathways can both converge on NAMPT. According to these data, NR would be converted to NAM by a nucleoside phosphorylase prior to the NAMPT catalyzed reaction (5,36). This is in keeping with the very low levels of NR kinase in the cytosol, as demonstrated by western blot and confocal microscopy.

Overall, our data provide a proof-of-principle of the validity of the use of organelle-specific biosensors to monitor NAD<sup>+</sup> fluctuations that occur in physio-pathological conditions. They also reinforce the concept of compartmentalization of NAD<sup>+</sup> biosynthesis, an essential aspect to understand how NAD<sup>+</sup> metabolism impacts on cancer cell metabolic adaptation. By offering a more complete picture of NAD<sup>+</sup> biosynthesis in MM, we aim to open the window of therapeutic strategies combining inhibitors of oncogenic signaling and of NAD<sup>+</sup> biosynthesis.

Gaudino F., et al.

## Innovation

In this study we used genetically encoded NAD<sup>+</sup> biosensors to dynamically characterize subcellular NAD<sup>+</sup> biosynthesis in intact BRAF-mutated metastatic melanoma (MM) cells. The choice of this model derives from our previous studies showing that melanoma transformation is accompanied by dysregulation of NAD<sup>+</sup> biosynthesis, which may be therapeutically targeted. By using organelle specific biosensors, we monitored NAD<sup>+</sup> fluctuations in response to biosynthetic precursors or inhibitors. Together with subcellular localization data, these results offer a complete picture of NAD<sup>+</sup> biosynthesis in MM cells and open the way to the use of biosensors to understand the NADome architecture in physio-pathological conditions.



1  
2  
3  
4  
5  
6  
7  
8  
9  
10  
11  
12  
13  
14  
15  
16  
17  
18  
19  
20  
21  
22  
23  
24  
25  
26  
27  
28  
29  
30  
31  
32  
33  
34  
35  
36  
37  
38  
39  
40  
41  
42  
43  
44  
45  
46  
47  
48  
49  
50  
51  
52  
53  
54  
55  
56  
57  
58  
59  
60

**Material and Methods**

**CpVenus-based NAD<sup>+</sup> sensor construct**

The NAD<sup>+</sup> biosensor is a chimeric molecule, composed by a circularly permuted Venus (cpVenus) fluorescent protein linked to a bipartite NAD<sup>+</sup>-binding domain of a bacterial DNA ligase (LigA1b and LigA1a) (9,15,19). Cytosolic, nuclear and mitochondrial biosensor expression vectors were kindly provided by X.A. Cambronne (Department of Molecular Biosciences, University of Texas, Austin, USA).

The incorporation of specific targeting sequences (CTGCAGAAAAAGCTGGAAGAGCTGGAAGTGGAC for cytosol, ATGCTGGCCACCCGCGTGTTCAGCCTGGTGGGCAAGCGCGCCATCAGCACCAGCGTGTGCGT GCGCGCCAC for mitochondria, and CCAAAGAAGAAGCGTAAGGTA for nuclei), allows these biosensors to be expressed in an organelle-specific way. DNA was amplified, incorporated in lentiviral particles (see below) and used for stable cell transduction. The LigA-cpVENUS biosensor presents two excitation peaks, one at 488 nm that decreases according to NAD<sup>+</sup> elevation and a second one at 405 nm that is unaffected by substrate variations, serving as internal control and system calibrator (9,15,19).

**Generation of lentivirus**

The vector plasmids (CMV-Sensor-IRES-puro-5 µg) together with third generation packaging plasmids (pMDL-2µg, pRSV-Rev-2µg, and the VSVG envelope encoding plasmid-1.2 µg, all from Addgene) were used for 293T cells transfection by using commercial Effectene transfection system (Quiagen, Milan, Italy, cod. 301425). After 48h, supernatants were collected, cells debris excluded (centrifugation at 600 x g for 5 minutes), and lentiviral particles concentrated (ultracentrifugation at 121,603 g for two hours) and used for cell transduction.

**Generation of cell lines stably expressing biosensors**

Gaudino F., et al.

A375 BRAFV600E-mutated cell lines were from the American Type Culture Collection (ATCC). BRAFi-resistant (BiR) variants were generated as described (2). Cells expressing cytosolic, nuclear or mitochondrial biosensors were obtained by transducing both A375/sensitive (S) and /BiR cells with a lentiviral vector carrying the specific organelle-targetable biosensor or with the organelle-targetable cpVENUS alone, using polybrene (8ug/ml; Sigma, Milan, Italy, cod. H9268). cpVENUS positive cells were flow sorted (FACS Aria III, BD Biosciences, Milan, Italy) and used as reported.

### Cell treatments

A375/S and /BiR lines were cultured in RPMI-1640 (Sigma, cod. R6504) with 10% of fetal calf serum (FCS) (Sigma, cod. F7524) and 10 IU/ml of penicillin / streptomycin (Sigma, cod. P4333). Cells were exposed to the following treatments for 16 hours. For NAMPT inhibition, cells were treated with 25 nM FK866 (Sigma, cod. F8557). Treatments with NAD<sup>+</sup> precursors were with 500 μM NMN (cod. N3501), 6 μM NA (cod. N4126), 0.5 μM NAM (cod. N3376), 200 μM QA (cod. P63204 all from Sigma) and 100 μM NR (kind gift of ChromaDex, Irvine, CA).

### Flow cytometry analysis

For flow cytometry analysis, cells were trypsinized (Sigma, cod. T4049) and collected in RPMI 10% FCS. Sensor/cpVenus FITC (excitation 488 nm, emission 530/30 nm) and BV510 (excitation 405 nm, emission 525/50 nm) were measured by flow cytometry (BD FACS Celesta) and data processed with DIVA version 8 (BD Biosciences) and FlowJo version 10.01 softwares (TreeStar, Ashland, OR). Cells were gated using forward scatter (FSC) and side scatter (SSC) for the live cells and then further gated on both SSC and FSC width to exclude doublets, analyzing at least 10<sup>4</sup> cells / sample. The analysis required a double ratio, expressed as a “ratio of ratios” (i.e. fold change). The first is the ratiometric 488/405 measurement detected by the biosensor, the second one is obtained by the parallel analysis of 488 nm/405 nm fluorescence changes of cells expressing the cpVENUS-only control (9,15,19). The cpVENUS 488/405 nm fluorescence ratio is used to normalize for NAD<sup>+</sup> changes

Gaudino F., et al.

independent of the biosensor. F0 refers to the ratio of ratios obtained in untreated conditions (F0=1). NAD<sup>+</sup> variations are finally expressed as the inverse relationship between the “ratio of ratios” changes and the cofactor concentrations. A “ratio of ratios” value >1 indicates decreased NAD<sup>+</sup> concentrations, while values <1 indicate increased levels of NAD<sup>+</sup>.

**Calibration curves**

Calibration curves of cytosolic and nuclear biosensors were generated as previously described (9). In details, cells expressing correspondent biosensors were permeabilized with saponin (0.005%), in the presence of propidium iodide (PI)(Sigma cod.P4170). Permeabilization status was monitored by looking at the percentage of PI positive cells. For mitochondrial biosensor-expressing cells, cells were first permeabilized for 10 minutes with saponin 0.005% and then treated with alamethicin (Sigma, cod. A4665) 30ug/ml in order to obtain mitochondria permeabilization and NAD<sup>+</sup> exchange through the organelle. Permeabilized cells were exposed to increasing concentrations (from 0 to 4 mM for cytosol and nuclei and from 0 to 10 mM for mitochondria) of exogenous NAD<sup>+</sup> (Sigma, cod. N-1511-1G). The NAD<sup>+</sup>-dependent fluorescence changes were monitored by flow cytometry. Each point composing the curve is the result of the ratio between 488nm and 405nm values of the biosensor normalized to the relative cpVENUS and lastly normalized on F0 (0 μM of NAD<sup>+</sup>).

**Mitochondria purification**

Mitochondria isolation was performed as previously described (21,32,63). Briefly, A375 cells (15x10<sup>7</sup>) cells were resuspended in IB<sub>c</sub> buffer (200mM sucrose, 1mM Tris-HCL, 1 mM EGTA, pH 7.4). Cells were mechanically disrupted by using an Elvehjem potter (Sigma, cod. P7734), and suspension was centrifuged (600 x g, 10 min, 4°C). This step was repeated twice to increase purification efficiency. Pellet was discarded and mitochondria-containing supernatant was centrifuged (8,000 x g, 10 min, 4°C). A centrifugation (8,500 x g, 10min, 4°C) on a discontinuous Percoll gradient (60, 30 and 18% Percoll, GE Healthcare, Milan, Italy, cod. GE17-0891-01), in IB<sub>c</sub> buffer, was used as last step

Gaudino F., et al.

of purification. The fraction between the 30% and 18% gradients was collected and washed three times by centrifugation at 19,000 x g for 10 min. Purified mitochondria were then lysed in a 1% NP-40 based buffer, subjected to Bradford quantification and prepared for western blot analysis with the same technical approach used for whole cell lysates (see below).

### Nuclei purification

Nuclei were isolated through a salt-based protocol and differential centrifugation steps. Cells ( $8 \times 10^6$ ) were collected from culture and resuspended in Buffer A (300 mM Sucrose, 10 mM Hepes, 10 mM KCl, 2 mM  $MgCl_2$ , 1 mM EGTA, KOH pH 7.9, complete of phosphatase and protease inhibitors). To lyse cells, NP-40 (0,15%) was added to the suspension, before centrifuging (1300 x g, 5 min) and the supernatant was centrifuged (16000 g, 15 min, 4°C) to eliminate membrane residues and used as cytosolic portion of the fractionating protocol. The pellet was then washed 5x in Buffer B (50 mM Hepes, 400 mM NaCl, 1 mM EDTA, pH 7.5 NAOH) (1300 g, 5 min) and subjected to 5 sonication steps. Finally, the suspension was centrifuged (130000 g for 15 min) and the obtained supernatant used as pure nuclear protein fraction.

### Western blot analysis

Whole cells or subcellular fractions obtained as described above, were resolved by SDS-PAGE, and transferred to nitrocellulose filter membranes (Biorad, Milan, cod. 1704158) (2). After blocking (5% Not-fat dry milk, Santa Cruz Biotechnology, Heidelberg, Germany, cod. sc2325), membranes were incubated with: anti-GFP (Cell Signaling Technologies, Danvers, MA, cod 2555S), anti-vinculin (Abcam, Cambridge, UK, cod. 130007), -tubulin (Cell Signaling Technologies, cod.2114), -actin (Santa Cruz Biotechnology, cod. sc-47778), -Hadha (Abcam, cod. 203114), -cytochrome C (BD Bioscience, cod. 556433), -H2A (Abcam, cod. ab18255), anti-NAMPT (Bethyl Laboratories, Montgomery, TX A300-779A), anti-NAPRT1 (Novus Biologicals, Cambridge, UK, cod. NBP1-87243), anti-C9orf95 (NRK1, ab169548) and anti-QPRT (ab57125 both from Abcam). After incubation with horseradish

Gaudino F., et al.

peroxidase-conjugated secondary antibody (PerkinElmer, Milan, Italy, cod. NEF822001EA), reaction was visualized with ECL (Biorad, cod. 1705061) using ImageQuant LAS4000 (GE Healthcare, Milan, Italy).

### Confocal microscopy

Cells expressing organelle-specific biosensors were cultured on glass cover slips in 24-well plates, rinsed once with PBS, fixed (4% PFA, 10 minutes, room temperature), permeabilized (0.1% saponin in PBS, 20 minutes, room temperature) and saturated with pre-immune goat serum (1:100, 1 hour, 4 °C). For NBEs localization studies, after saturation cells were incubated with primary antibodies: anti-NAMPT, anti-NAPRT1, anti-C9orf95 and anti-QPRT, anti-TOM20 (cod. SC-11415 from Santa Cruz Biotechnology). MitoTracker Deep Red (ThermoFischer, cod. M22426). was used for mitochondria staining. TCS SP5 laser scanning confocal microscope equipped with an oil immersion 63X objective, was used for fluorescence acquisition. Images were acquired with LAS AF software (Leica Microsystem), files were processed with Photoshop (Adobe Systems, San Jose, CA) and pixel intensity was calculated using the ImageJ software (<http://rsbweb.nih.gov/ij/>).

### Time lapse analysis

For time lapse imaging, A375 (12X10<sup>5</sup>) were cultured into a  $\mu$ -Slide 4 well Ibidi Chambered coverslips (Ibidi, Giemme Snc, Milan, Italy, cod. 80426), in RPMI-1640 with 10% of FCS. TCS SP5 was also equipped for maintaining cells under physiological conditions (5% CO<sub>2</sub> and 37°C). for the duration of the experiments. At time 0 (t=0) cells were treated with FK866 25 nM, for a period of 6 hours. Time lapse series were acquired with 10 minutes intervals for mitochondrial and nuclear biosensor, for 5 minutes for cytosolic biosensor, between successive frames. To obtain the full cell thickness, for each acquisition field, different z-stacks were acquired and the sum of z stacks obtained with ImageJ software analysis was used for video generation. Finally, the ImageJ plugin "image

Gaudino F., et al.

calculator'' was used to obtain the values of fluorescence ratio between 488nm and 405nm channels.

### Statistical analysis

Statistical analyses were performed with GraphPad version 6.0 (GraphPad Software Inc., La Jolla, CA). Data were analyzed by two-sided paired Student's t test. Results are reported as box plots, where the top and bottom margins of the box define the 25th and 75th percentiles, the line in the box defines the median, and the error bars define the minimum and maximum of all data. *P* value<.05 was considered to be statistically significant.

1 *Gaudino F., et al.*

2

3 **Acknowledgements**

4

5 Thanks are given to Dr. Xiaolou Cambronne (University of Austin, TX) for providing the constructs,

6

7

8 to Dr. Marta Gai (University of Turin, Turin Italy) for assistance in the use of the confocal microscope

9

10 and in data analysis and to Dr. Ambra Grolla (University of Eastern Piedmont, Novara, Italy) for

11

12 providing protocols for nuclei isolation. Experiments were performed in the laboratories of the

13

14

15 Italian Institute for Genomic Medicine (IIGM).

16

17

18

19

20

21

22

23

24

25

26

27

28

29

30

31

32

33

34

35

36

37

38

39

40

41

42

43

44

45

46

47

48

49

50

51

52

53

54

55

56

57

58

59

60

Gaudino F., et al.

## Abbreviations Used

**A375/S** = A375 sensitive to BRAF inhibitors

**A375/BiR** = A375 resistant to BRAF inhibitors

**AlaM** = alamethicin

**ARTs** = adenosine diphosphate (ADP)-ribose transferases

**BRAFi** = BRAF inhibitor

**cpVENUS** = circularly permuted Venus protein

**ETC** = electron transport chain

**GDP6** = glucose-6-phosphate dehydrogenase

**GR** = glutathione reductase

**GSH** = glutathione

**GSSG** = oxidized glutathione

**HPLC** = high performance liquid chromatography

**MM** = metastatic melanoma

**NA** = nicotinic acid

**NAD<sup>+</sup>** = nicotinamide adenine dinucleotide

**NADH** = reduced nicotinamide adenine dinucleotide

**NADP** = nicotinamide adenine dinucleotide phosphate

**NADPH** = reduced nicotinamide adenine dinucleotide phosphate

**NAM** = nicotinamide

**NaMN** = nicotinic acid mononucleotide

**NAMPT** = nicotinamide phosphoribosyltransferase

**NAMPTis** = nicotinamide phosphoribosyltransferase inhibitors

**NAPRT** = nicotinate phosphoribosyltransferase



1 *Gaudino F., et al.*

2  
3 **NBEs** = NAD<sup>+</sup> biosynthetic enzymes

4  
5 **Ndt1p** = mitochondrial NAD<sup>+</sup> carrier protein

6  
7  
8 **NMN** = nicotinamide mononucleotide

9  
10 **NMNAT** = nicotinamide mononucleotide adenylyltransferase

11  
12  
13 **NR** = nicotinamide riboside

14  
15 **NRK** = nicotinamide riboside kinase

16  
17 **PARPs** = poly (ADP-ribose) polymerases

18  
19 **PRPP** = phosphoribosylpyrophosphate

20  
21  
22 **QA** = quinolinic acid

23  
24  
25 **QPRT** = quinolinate phosphoribosyltransferase

26  
27 **SIRT**s = sirtuins

28  
29  
30 **TCA** = tricarboxylic acid cycle

31  
32 **TR** = thioredoxin reductase

33  
34  
35

36  
37  
38

39  
40  
41

42  
43  
44

45  
46  
47

48  
49  
50

51  
52  
53

54  
55  
56

57  
58  
59

60

Gaudino F., et al.

## References

1. Alano CC, Tran A, Tao R, Ying W, Karliner JS, Swanson RA. Differences among cell types in NAD(+) compartmentalization: a comparison of neurons, astrocytes, and cardiac myocytes. *J Neurosci Res* 85: 3378-85, 2007.
2. Audrito V, Manago A, La Vecchia S, Zamporlini F, Vitale N, Baroni G, Cignetto S, Serra S, Bologna C, Stingi A, Arruga F, Vaisitti T, Massi D, Mandala M, Raffaelli N, Deaglio S. Nicotinamide Phosphoribosyltransferase (NAMPT) as a Therapeutic Target in BRAF-Mutated Metastatic Melanoma. *J Natl Cancer Inst* 110, 2018.
3. Audrito V, Manago A, Zamporlini F, Rulli E, Gaudino F, Madonna G, D'Atri S, Antonini Cappellini GC, Ascierto PA, Massi D, Raffaelli N, Mandala M, Deaglio S. Extracellular nicotinamide phosphoribosyltransferase (eNAMPT) is a novel marker for patients with BRAF-mutated metastatic melanoma. *Oncotarget* 9: 18997-19005, 2018.
4. Batandier C, Leverve X, Fontaine E. Opening of the mitochondrial permeability transition pore induces reactive oxygen species production at the level of the respiratory chain complex I. *J Biol Chem* 279: 17197-204, 2004.
5. Belenky P, Christensen KC, Gazzaniga F, Pletnev AA, Brenner C. Nicotinamide riboside and nicotinic acid riboside salvage in fungi and mammals. Quantitative basis for Urh1 and purine nucleoside phosphorylase function in NAD<sup>+</sup> metabolism. *J Biol Chem* 284: 158-64, 2009.
6. Bender DA. Biochemistry of tryptophan in health and disease. *Mol Aspects Med* 6: 101-97, 1983.
7. Berger F, Lau C, Dahlmann M, Ziegler M. Subcellular compartmentation and differential catalytic properties of the three human nicotinamide mononucleotide adenylyltransferase isoforms. *J Biol Chem* 280: 36334-41, 2005.

Gaudino F., et al.

8. Bitterman KJ, Anderson RM, Cohen HY, Latorre-Esteves M, Sinclair DA. Inhibition of silencing and accelerated aging by nicotinamide, a putative negative regulator of yeast sir2 and human SIRT1. *J Biol Chem* 277: 45099-107, 2002.
9. Cambronne XA, Stewart ML, Kim D, Jones-Brunette AM, Morgan RK, Farrens DL, Cohen MS, Goodman RH. Biosensor reveals multiple sources for mitochondrial NAD(+). *Science* 352: 1474-7, 2016.
10. Canto C, Menzies KJ, Auwerx J. NAD(+) Metabolism and the Control of Energy Homeostasis: A Balancing Act between Mitochondria and the Nucleus. *Cell Metab* 22: 31-53, 2015.
11. Cerna D, Li H, Flaherty S, Takebe N, Coleman CN, Yoo SS. Inhibition of nicotinamide phosphoribosyltransferase (NAMPT) activity by small molecule GMX1778 regulates reactive oxygen species (ROS)-mediated cytotoxicity in a p53- and nicotinic acid phosphoribosyltransferase1 (NAPRT1)-dependent manner. *J Biol Chem* 287: 22408-17, 2012.
12. Chiarugi A, Dolle C, Felici R, Ziegler M. The NAD metabolome--a key determinant of cancer cell biology. *Nat Rev Cancer* 12: 741-52, 2012.
13. Chio IIC, Tuveson DA. ROS in Cancer: The Burning Question. *Trends Mol Med* 23: 411-429, 2017.
14. Chowdhry S, Zanca C, Rajkumar U, Koga T, Diao Y, Raviram R, Liu F, Turner K, Yang H, Brunk E, Bi J, Furnari F, Bafna V, Ren B, Mischel PS. NAD metabolic dependency in cancer is shaped by gene amplification and enhancer remodelling. *Nature* 569: 570-575, 2019.
15. Cohen MS, Stewart ML, Goodman RH, Cambronne XA. Methods for Using a Genetically Encoded Fluorescent Biosensor to Monitor Nuclear NAD<sup>+</sup>. *Methods Mol Biol* 1813: 391-414, 2018.
16. Connell NJ, Houtkooper RH, Schrauwen P. NAD(+) metabolism as a target for metabolic health: have we found the silver bullet? *Diabetologia*, 2019.

Gaudino F., et al.

17. Davila A, Liu L, Chellappa K, Redpath P, Nakamaru-Ogiso E, Paoletta LM, Zhang Z, Migaud ME, Rabinowitz JD, Baur JA. Nicotinamide adenine dinucleotide is transported into mammalian mitochondria. *Elife* 7, 2018.
18. Di Stefano M, Conforti L. Diversification of NAD biological role: the importance of location. *FEBS J* 280: 4711-28, 2013.
19. Eller JM, Stewart ML, Slepian AJ, Markwardt S, Wiedrick J, Cohen MS, Goodman RH, Cambronne XA. Flow Cytometry Analysis of Free Intracellular NAD(+) Using a Targeted Biosensor. *Curr Protoc Cytom* 88: e54, 2019.
20. Felici R, Lapucci A, Ramazzotti M, Chiarugi A. Insight into molecular and functional properties of NMNAT3 reveals new hints of NAD homeostasis within human mitochondria. *PLoS One* 8: e76938, 2013.
21. Frezza C, Cipolat S, Scorrano L. Organelle isolation: functional mitochondria from mouse liver, muscle and cultured fibroblasts. *Nat Protoc* 2: 287-95, 2007.
22. Garten A, Schuster S, Penke M, Gorski T, de Giorgis T, Kiess W. Physiological and pathophysiological roles of NAMPT and NAD metabolism. *Nat Rev Endocrinol* 11: 535-46, 2015.
23. Gostimskaya IS, Grivennikova VG, Zharova TV, Bakeeva LE, Vinogradov AD. In situ assay of the intramitochondrial enzymes: use of alamethicin for permeabilization of mitochondria. *Anal Biochem* 313: 46-52, 2003.
24. Green RM, Graham M, O'Donovan MR, Chipman JK, Hodges NJ. Subcellular compartmentalization of glutathione: correlations with parameters of oxidative stress related to genotoxicity. *Mutagenesis* 21: 383-90, 2006.

Gaudino F., et al.

25. Grozio A, Sociali G, Sturla L, Caffa I, Soncini D, Salis A, Raffaelli N, De Flora A, Nencioni A, Bruzzone S. CD73 protein as a source of extracellular precursors for sustained NAD<sup>+</sup> biosynthesis in FK866-treated tumor cells. *J Biol Chem* 288: 25938-49, 2013.
26. Hasmann M, Schemainda I. FK866, a highly specific noncompetitive inhibitor of nicotinamide phosphoribosyltransferase, represents a novel mechanism for induction of tumor cell apoptosis. *Cancer Res* 63: 7436-42, 2003.
27. Hassinen IE. Signaling and Regulation Through the NAD(+) and NADP(+) Networks. *Antioxid Redox Signal* 30: 857-874, 2019.
28. Holen K, Saltz LB, Hollywood E, Burk K, Hanauske AR. The pharmacokinetics, toxicities, and biologic effects of FK866, a nicotinamide adenine dinucleotide biosynthesis inhibitor. *Invest New Drugs* 26: 45-51, 2008.
29. Houtkooper RH, Canto C, Wanders RJ, Auwerx J. The secret life of NAD<sup>+</sup>: an old metabolite controlling new metabolic signaling pathways. *Endocr Rev* 31: 194-223, 2010.
30. Koch-Nolte F, Fischer S, Haag F, Ziegler M. Compartmentation of NAD<sup>+</sup>-dependent signalling. *FEBS Lett* 585: 1651-6, 2011.
31. Kulkarni CA, Brookes P. Cellular Compartmentation and the Redox/Non-Redox Functions of NAD<sup>+</sup>. *Antioxid Redox Signal*, 2019.
32. Leanza L, Henry B, Sassi N, Zoratti M, Chandy KG, Gulbins E, Szabo I. Inhibitors of mitochondrial Kv1.3 channels induce Bax/Bak-independent death of cancer cells. *EMBO Mol Med* 4: 577-93, 2012.
33. Liou GY, Storz P. Reactive oxygen species in cancer. *Free Radic Res* 44: 479-96, 2010.
34. Magni G, Amici A, Emanuelli M, Orsomando G, Raffaelli N, Ruggieri S. Enzymology of NAD<sup>+</sup> homeostasis in man. *Cell Mol Life Sci* 61: 19-34, 2004.

Gaudino F., et al.

35. Maldi E, Travelli C, Caldarelli A, Agazzone N, Cintura S, Galli U, Scatolini M, Ostano P, Miglino B, Chiorino G, Boldorini R, Genazzani AA. Nicotinamide phosphoribosyltransferase (NAMPT) is over-expressed in melanoma lesions. *Pigment Cell Melanoma Res* 26: 144-6, 2013.
36. Martens CR, Denman BA, Mazzo MR, Armstrong ML, Reisdorph N, McQueen MB, Chonchol M, Seals DR. Chronic nicotinamide riboside supplementation is well-tolerated and elevates NAD(+) in healthy middle-aged and older adults. *Nat Commun* 9: 1286, 2018.
37. Matic S, Geisler DA, Moller IM, Widell S, Rasmusson AG. Alamethicin permeabilizes the plasma membrane and mitochondria but not the tonoplast in tobacco (*Nicotiana tabacum* L. cv Bright Yellow) suspension cells. *Biochem J* 389: 695-704, 2005.
38. Montecucco F, Bauer I, Braunersreuther V, Bruzzone S, Akhmedov A, Luscher TF, Speer T, Poggi A, Mannino E, Pelli G, Galan K, Bertolotto M, Lenglet S, Garuti A, Montessuit C, Lerch R, Pellioux C, Vuilleumier N, Dallegrì F, Mage J, Sebastian C, Mostoslavsky R, Gayet-Ageron A, Patrone F, Mach F, Nencioni A. Inhibition of nicotinamide phosphoribosyltransferase reduces neutrophil-mediated injury in myocardial infarction. *Antioxid Redox Signal* 18: 630-41, 2013.
39. Morgan B, Ezerina D, Amoako TN, Riemer J, Seedorf M, Dick TP. Multiple glutathione disulfide removal pathways mediate cytosolic redox homeostasis. *Nat Chem Biol* 9: 119-25, 2013.
40. Nikiforov A, Dolle C, Niere M, Ziegler M. Pathways and subcellular compartmentation of NAD biosynthesis in human cells: from entry of extracellular precursors to mitochondrial NAD generation. *J Biol Chem* 286: 21767-78, 2011.
41. Palmieri F, Rieder B, Ventrella A, Blanco E, Do PT, Nunes-Nesi A, Trauth AU, Fiermonte G, Tjaden J, Agrimi G, Kirchberger S, Paradies E, Fernie AR, Neuhaus HE. Molecular identification

Gaudino F., et al.

- and functional characterization of *Arabidopsis thaliana* mitochondrial and chloroplastic NAD<sup>+</sup> carrier proteins. *J Biol Chem* 284: 31249-59, 2009.
42. Piacente F, Caffa I, Ravera S, Sociali G, Passalacqua M, Vellone VG, Becherini P, Reverberi D, Monacelli F, Ballestrero A, Odetti P, Cagnetta A, Cea M, Nahimana A, Duchosal M, Bruzzone S, Nencioni A. Nicotinic Acid Phosphoribosyltransferase Regulates Cancer Cell Metabolism, Susceptibility to NAMPT Inhibitors, and DNA Repair. *Cancer Res* 77: 3857-3869, 2017.
43. Pirinen E, Canto C, Jo YS, Morato L, Zhang H, Menzies KJ, Williams EG, Mouchiroud L, Moullan N, Hagberg C, Li W, Timmers S, Imhof R, Verbeek J, Pujol A, van Loon B, Viscomi C, Zeviani M, Schrauwen P, Sauve AA, Schoonjans K, Auwerx J. Pharmacological Inhibition of poly(ADP-ribose) polymerases improves fitness and mitochondrial function in skeletal muscle. *Cell Metab* 19: 1034-41, 2014.
44. Pittelli M, Felici R, Pitozzi V, Giovannelli L, Bigagli E, Cialdai F, Romano G, Moroni F, Chiarugi A. Pharmacological effects of exogenous NAD on mitochondrial bioenergetics, DNA repair, and apoptosis. *Mol Pharmacol* 80: 1136-46, 2011.
45. Raffaelli N, Sorci L, Amici A, Emanuelli M, Mazzola F, Magni G. Identification of a novel human nicotinamide mononucleotide adenylyltransferase. *Biochem Biophys Res Commun* 297: 835-40, 2002.
46. Rajman L, Chwalek K, Sinclair DA. Therapeutic Potential of NAD-Boosting Molecules: The In Vivo Evidence. *Cell Metab* 27: 529-547, 2018.
47. Ratajczak J, Joffraud M, Trammell SA, Ras R, Canela N, Boutant M, Kulkarni SS, Rodrigues M, Redpath P, Migaud ME, Auwerx J, Yanes O, Brenner C, Canto C. NRK1 controls nicotinamide mononucleotide and nicotinamide riboside metabolism in mammalian cells. *Nat Commun* 7: 13103, 2016.

Gaudino F., et al.

48. Revollo JR, Grimm AA, Imai S. The NAD biosynthesis pathway mediated by nicotinamide phosphoribosyltransferase regulates Sir2 activity in mammalian cells. *J Biol Chem* 279: 50754-63, 2004.
49. Revollo JR, Grimm AA, Imai S. The regulation of nicotinamide adenine dinucleotide biosynthesis by Nampt/PBEF/visfatin in mammals. *Curr Opin Gastroenterol* 23: 164-70, 2007.
50. Sallin O, Reymond L, Gondrand C, Raith F, Koch B, Johnsson K. Semisynthetic biosensors for mapping cellular concentrations of nicotinamide adenine dinucleotides. *Elife* 7, 2018.
51. Sauve AA, Wolberger C, Schramm VL, Boeke JD. The biochemistry of sirtuins. *Annu Rev Biochem* 75: 435-65, 2006.
52. Shackelford RE, Mayhall K, Maxwell NM, Kandil E, Coppola D. Nicotinamide phosphoribosyltransferase in malignancy: a review. *Genes Cancer* 4: 447-56, 2013.
53. Sharif T, Martell E, Dai C, Ghassemi-Rad MS, Kennedy BE, Lee PWK, Gujar S. Regulation of Cancer and Cancer-Related Genes via NAD(). *Antioxid Redox Signal*, 2018.
54. Stein LR, Imai S. The dynamic regulation of NAD metabolism in mitochondria. *Trends Endocrinol Metab* 23: 420-8, 2012.
55. Todisco S, Agrimi G, Castegna A, Palmieri F. Identification of the mitochondrial NAD<sup>+</sup> transporter in *Saccharomyces cerevisiae*. *J Biol Chem* 281: 1524-31, 2006.
56. Trammell SA, Schmidt MS, Weidemann BJ, Redpath P, Jaksch F, Dellinger RW, Li Z, Abel ED, Migaud ME, Brenner C. Nicotinamide riboside is uniquely and orally bioavailable in mice and humans. *Nat Commun* 7: 12948, 2016.
57. Verdin E. NAD(+) in aging, metabolism, and neurodegeneration. *Science* 350: 1208-13, 2015.
58. von Heideman A, Berglund A, Larsson R, Nygren P. Safety and efficacy of NAD depleting cancer drugs: results of a phase I clinical trial of CHS 828 and overview of published data. *Cancer Chemother Pharmacol* 65: 1165-72, 2010.



Gaudino F., et al.

59. Xiao W, Wang RS, Handy DE, Loscalzo J. NAD(H) and NADP(H) Redox Couples and Cellular Energy Metabolism. *Antioxid Redox Signal* 28: 251-272, 2018.
60. Xu TY, Zhang SL, Dong GQ, Liu XZ, Wang X, Lv XQ, Qian QJ, Zhang RY, Sheng CQ, Miao CY. Discovery and characterization of novel small-molecule inhibitors targeting nicotinamide phosphoribosyltransferase. *Sci Rep* 5: 10043, 2015.
61. Yang H, Yang T, Baur JA, Perez E, Matsui T, Carmona JJ, Lamming DW, Souza-Pinto NC, Bohr VA, Rosenzweig A, de Cabo R, Sauve AA, Sinclair DA. Nutrient-sensitive mitochondrial NAD<sup>+</sup> levels dictate cell survival. *Cell* 130: 1095-107, 2007.
62. Ying W. NAD<sup>+</sup>/NADH and NADP<sup>+</sup>/NADPH in cellular functions and cell death: regulation and biological consequences. *Antioxid Redox Signal* 10: 179-206, 2008.
63. Zaccagnino A, Manago A, Leanza L, Gontarewitz A, Linder B, Azzolini M, Biasutto L, Zoratti M, Peruzzo R, Legler K, Trauzold A, Kalthoff H, Szabo I. Tumor-reducing effect of the clinically used drug clofazimine in a SCID mouse model of pancreatic ductal adenocarcinoma. *Oncotarget* 8: 38276-38293, 2017.
64. Zhang M, Ying W. NAD(+) Deficiency Is a Common Central Pathological Factor of a Number of Diseases and Aging: Mechanisms and Therapeutic Implications. *Antioxid Redox Signal* 30: 890-905, 2019.
65. Zhao Y, Zhang Z, Zou Y, Yang Y. Visualization of Nicotine Adenine Dinucleotide Redox Homeostasis with Genetically Encoded Fluorescent Sensors. *Antioxid Redox Signal* 28: 213-229, 2018.

**Figures Legends**

**Figure 1. Generation of A375 cells stably expressing organelle-specific NAD<sup>+</sup> biosensors**

Gaudino F., et al.

(A,B,C) Confocal microscopy : cells were cultured on glass cover slips in 24-well plates, fixed (4% PFA), permeabilized (0.1% saponin) and saturated with pre-immune goat serum. Cells were counterstained with phalloidin (red), TOM20 (magenta) and DAPI (blue) to highlight cytosol, mitochondria and nuclei, respectively. Fluorescence was acquired by confocal microscopy, using an oil immersion 63x objective. Slides were analyzed using a TCS SP5 laser scanning confocal microscope; images were acquired with LAS AF software Scale bar= 25 $\mu$ m for cytosolic A375 S/BiR, nuclear A375 S/BiR and mitochondrial A375/BiR; Scale bar= 10 $\mu$ m for mitochondrial A375/S. Diagrams on the top of each panel show the structure of the different constructs. A375/S : A375 sensitive to BRAF inhibitors; A375/BiR : A375 resistant to BRAF inhibitors.

## Figure 2. Effects of the NAMPT inhibitor FK866

(A) Upper: quantification of time lapse imaging of A375 cells expressing the cytosolic, mitochondrial and nuclear biosensor, in response to FK866 (25nM, 4h period). Cells were cultured on Ibidi chambered coverslips and kept at 5% CO<sub>2</sub> and 37°C during the experiment. Curves show the fluorescence ratio between 488 nm and 405 nm of the biosensor reported as a function of time. 488 nm and 405 nm fluorescence were separately recorded and the ratio was obtained by image calculator plugin of ImageJ software analysis. Curves are the results of 4 independent measurements. Lower: representative frames of A375 expressing relative biosensors at time (t) =0 and t=4. Fluorescence was acquired by confocal microscopy, using an oil immersion 63x objective, in the figure A cropped images from zoomed acquisition fields are shown. NAD<sup>+</sup> depletion can be followed by observing the increase of fluorescence intensity (movies 1-2-3). (B) NAD<sup>+</sup> variations measured in A375 cytosol (C), mitochondria (M) and nuclei (N) after treatment with FK866 (25 nM, 16 hours). Box plots are the results of 9 different experiments. Results are expressed as a "Ratio of Ratio" [F488/405(S/cpV)/F0]. Sensor/cpVenus (488 nm/405 nm) fluorescence ratios were measured by flow cytometry and the fold change compared with untreated controls (F0). (C) Representative

Gaudino F., et al.

example of fluorescence variation of the cytosolic biosensor upon FK866 treatment in A375. Dot plot (on the left) and histogram (on the right) show the specificity of the NAMPT inhibitor -induced NAD<sup>+</sup> depletion in increasing biosensor 488 nm fluorescence. UN: untreated.

**Figure 3. Subcellular NAD<sup>+</sup> concentrations and effects of NMN on subcellular NAD<sup>+</sup> levels**

(A) Calibration curve of cytosolic, mitochondrial and nuclear biosensors obtained in A375. Cells were permeabilized with 0,005% saponin (cytosolic and nuclear biosensors) or with saponin and Alamethicin (mitochondrial biosensor expressing A375) and exposed to increased exogenous concentrations of NAD<sup>+</sup>. The fluorescence ratios (488 nm/405 nm) of the biosensor were normalized to cpVENUS. Diagrams show normalized fluorescence ratios (y-axis) reported as a function of logarithmic NAD<sup>+</sup> concentrations (x-axis) and fit with a variable slope model. Curves are the results of 4 independent experiments.(B) Intracellular NAD<sup>+</sup> variations in A375 after treatment with NMN (0.5 mM, 16 hours), in presence or absence of FK866 25 nM (n=5). Results are expressed as a “Ratio of Ratio” [F488/405(S/coV)/F0]. Sensor/cpVenus (488 nm/405 nm) fluorescence ratios were measured by flow cytometry and the fold change was compared to untreated controls (F0). Two-sided paired Student’s t test was used to determine statistical significance. Star marks refer to the significance of the relative change of each treatments condition compared to the untreated (untreated=1), while the *p* value refers to the rescue of supplementations from the FK866-treated condition. Boxes represent interquartile range, and the horizontal line across each box indicates the median. ns= not statistically significant.

**Figure 4. Topography of NAD<sup>+</sup> Biosynthesis: NAM and NA primarily affect cytosolic NAD<sup>+</sup> levels**

Cells were treated as follows: (A) 500 μM NAM ± 25 nM FK866; (B) 6 μM NA ± 25 nM FK866. Results are expressed as a “Ratio of Ratio” [F488/405(S/coV)/F0]. Sensor/cpVenus (488 nm/405 nm) fluorescence ratios were measured by flow cytometry and the fold change was compared to untreated controls (F0) (n=5). Star marks refer to the significance of the relative change of each

Gaudino F., et al.

treatments condition compared to the untreated (untreated=1), while the  $p$  value refers to the rescue of supplementations from the FK866-treated condition.

#### **Figure 5. Topography of NAD<sup>+</sup> Biosynthesis: NR and QA showed an organelle-specific impact on NAD<sup>+</sup> levels**

Cells were treated with (C) 100  $\mu$ M NR  $\pm$  25 nM FK866; (D) 200  $\mu$ M QA  $\pm$  25 nM FK866. A375 cells were exposed to the treatments for 16 hours. Results are expressed as a "Ratio of Ratio" [F488/405(S/coV)/F0]. Sensor/cpVenus (488 nm/405 nm) fluorescence ratios were measured by flow cytometry and the fold change was compared to untreated controls (F0) (n=5). Star marks refer to the significance of the relative change of each treatments condition compared to the untreated (untreated=1), while the  $p$  value refers to the rescue of supplementations from the FK866-treated condition.

#### **Figure 6. Subcellular localization of NAD<sup>+</sup> biosynthetic enzymes**

(A) Mitochondria and nuclei were isolated as described in material and methods. 10 $\mu$ g of each lysate were loaded in the following order: whole cell lysate (WCL), cytosolic fraction (C), mitochondrial fraction (M) and nuclear fraction (N). Anti-Vinculin, anti-tubulin, anti-actin, anti-Hadha, anti-cytochrome c and anti-H2A were used to determine the purity of cytosolic, mitochondrial and nuclear fractions, respectively. (B) Graph represents the percentage of NBEs expression in each fraction. Band quantification was performed using ImageQuant software. Values are referred to the mean of 6 independent experiments. % was calculated as: % of pixel intensity of district specific band/sum of all districts pixel intensities. (C) On the left confocal microscopy showing NAMPT, NAPRT, NRK, QPRT total expression (green fluorescence) in whole cells (merge). Cytosol, mitochondria and nuclei were counterstained with phalloidin (red), MitoTracker (magenta) and DAPI (blue) respectively (zoomed image of 63X magnification, scale bar= 10 $\mu$ m). On the right NBEs-cytosol/mitochondria/nuclei sub-localization. In detail, NAMPT, NAPRT, NRK and QPRT (green

Gaudino F., et al.

fluorescence) were localized by delimiting fractions (red fluorescence) separately by using the co-localization tool of LAS AF Version Lite 2.4 software. Representative images show single NBE and single compartment overlapping (image of 63X magnification, scale bar= 25µm).

**Figure 7. A375/S and /BiR responses to the NAMPT inhibition**

Cytosolic, mitochondrial and nuclear NAD<sup>+</sup> variations were measured in BRAFi-sensitive (S) or resistant (BiR) cells after treatment with FK866 (25 nM, 16 hours). Results are expressed as relative fold change [F488/405(S/coV)/F0]. Sensor/cpVenus (488 nm/405 nm) fluorescence ratios were measured by flow cytometry and the fold change was compared to untreated (F0). Box plot representing 9 independent experiments. Star marks refers to the relative change of FK866 treatment compared to 1 (untreated), while p value indicates significance of the FK866 differential response of A375/BiR compared to A375/S.

**Figure 8. Compartmentalization of NAD<sup>+</sup> biosynthesis in A375 MM**

On the top schematic representation of biochemical reactions involved in NAD<sup>+</sup> production. NAD<sup>+</sup> precursors present in the extracellular space can enter the cell becoming substrates of the NBEs. QA enters in the *de novo* biosynthetic pathway, while NA, NR and NAM are substrates of the parallel three salvage pathways. Among the NAD<sup>+</sup> precursors NAM is also the by-product of NAD<sup>+</sup> consuming enzymes such as sirtuins and PARPs. NAM and NR can be used to produce NMN by NAMPT and NRKs, respectively. NMN and NaMN (produced by NAPRT-mediated Na conversion) are finally used by compartmentalized NMNATs to generate NAD<sup>+</sup>. In the center, an A375 melanoma cell acquired by using confocal microscope. Cytosol, mitochondria and nuclei were counterstained with phalloidin (red), MitoTracker (magenta) and DAPI (blue) respectively (zoomed image of 63X magnification acquired by confocal microscopy , a cropped image is shown). Insets of A375 cytosol, nucleus and mitochondria resume the most relevant NBEs found in each A375 subcellular districts. Enzymes written in bold are the most expressed NBEs in the highlighted cell districts, while percentage refers

Gaudino F., et al.

to the expression level of each enzymes in each compartment. The cytosolic picture of A375 NAD<sup>+</sup> biosynthesis is composed by a dominant cytosolic NAMPT pathway converting NAM into NMN. NAPRT can be considered a second, but highly active, enzyme which mediates the cytosolic NA conversion to NaMN, indeed its localization was found to be more than 92% cytosolic. These pathways contribute to the generation of an NAD<sup>+</sup> pool calculated to be around 261  $\mu$ M. In the nucleus, the NAD<sup>+</sup> pool is approximately 258  $\mu$ M and the primary expressed NBEs is NRK. In this compartment, we were also able to detect low levels of NAMPT and NAPRT (5.1% and 2% of their total expression, respectively). NRK expression is also prevalent in mitochondria (67.2 % of its total biochemical detection), where the calculated NAD<sup>+</sup> concentration is 499  $\mu$ M. In this organelle, low expression of NAMPT (10.74%) and NAPRT (5.7%) could contribute to the maintenance of mitochondrial NAD<sup>+</sup> pool.

**Table 1. Fluorescence variations of each biosensors in the presence of NAD<sup>+</sup>**

Table showing cpVENUS normalized fluorescence variations of each biosensors when exposed to increasing concentrations of exogenous NAD<sup>+</sup> in a condition of saponin or saponin/alamethicin-mediated permeabilization. Reported numbers are the mean of four independent experiments for cytosolic and nuclear biosensor, of three independent experiments for mitochondrial biosensor.



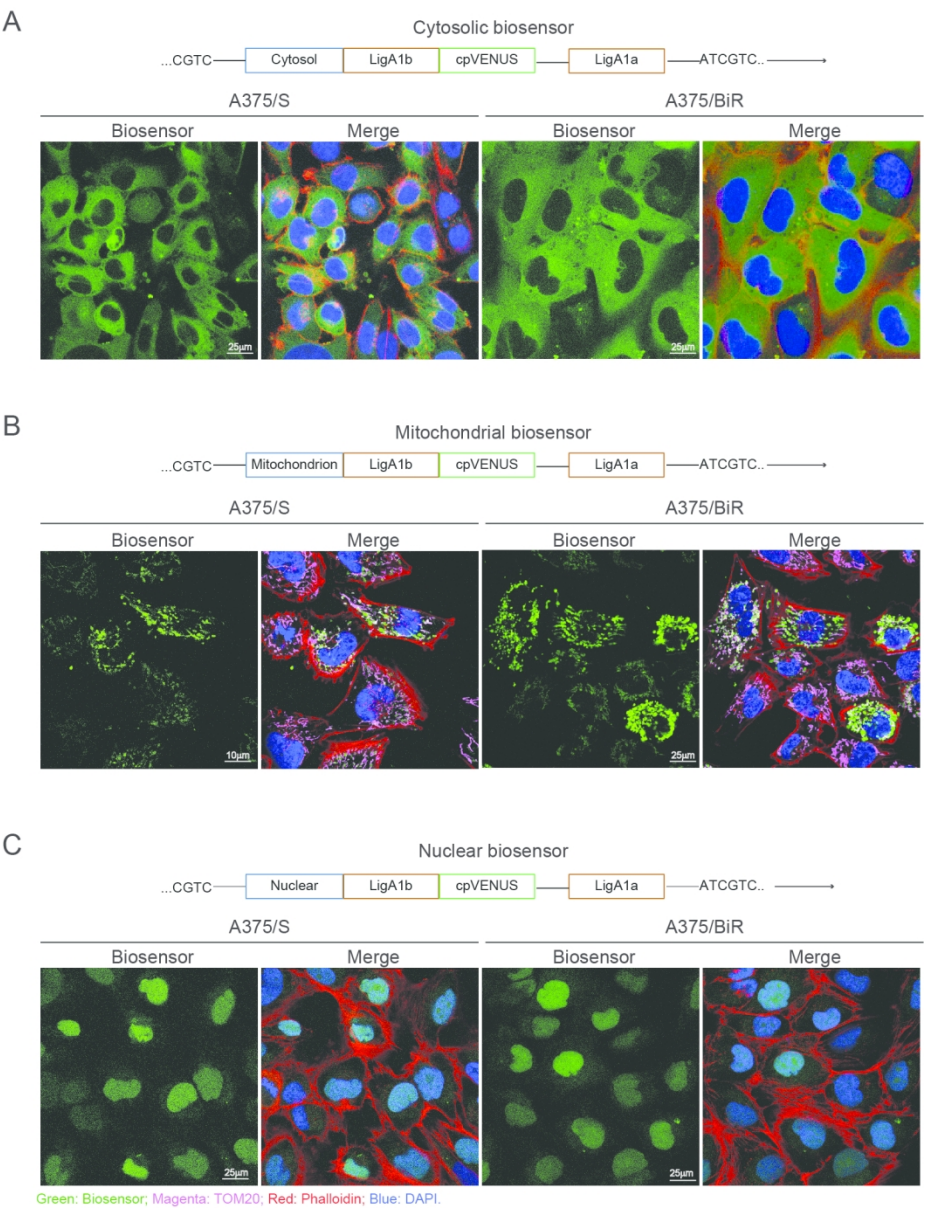


Figure 1. Generation of A375 cells stably expressing organelle-specific NAD<sup>+</sup> biosensors (A,B,C) Confocal microscopy : cells were cultured on glass cover slips in 24-well plates, fixed (4% PFA), permeabilized (0.1% saponin) and saturated with pre-immune goat serum. Cells were counterstained with phalloidin (red), TOM20 (magenta) and DAPI (blue) to highlight cytosol, mitochondria and nuclei, respectively. Fluorescence was acquired by confocal microscopy, using an oil immersion 63x objective. Slides were analyzed using a TCS SP5 laser scanning confocal microscope; images were acquired with LAS AF software Scale bar= 25μm for cytosolic A375 S/BiR, nuclear A375 S/BiR and mitochondrial A375/BiR; Scale bar= 10μm for mitochondrial A375/S. Diagrams on the top of each panel show the structure of the different constructs. A375/S : A375 sensitive to BRAF inhibitors; A375/BiR : A375 resistant to BRAF inhibitors.

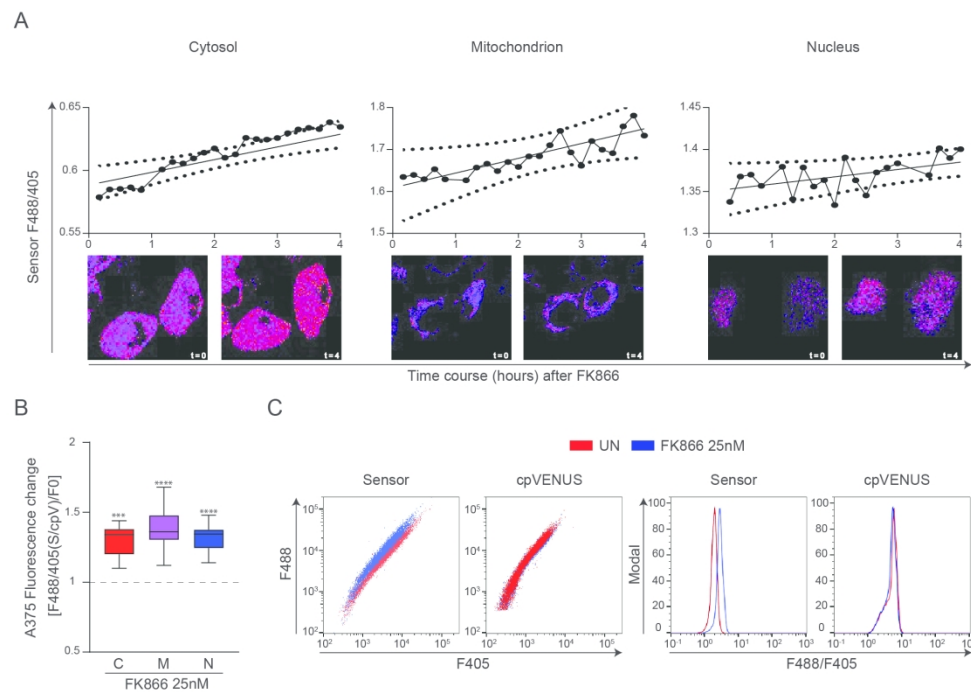
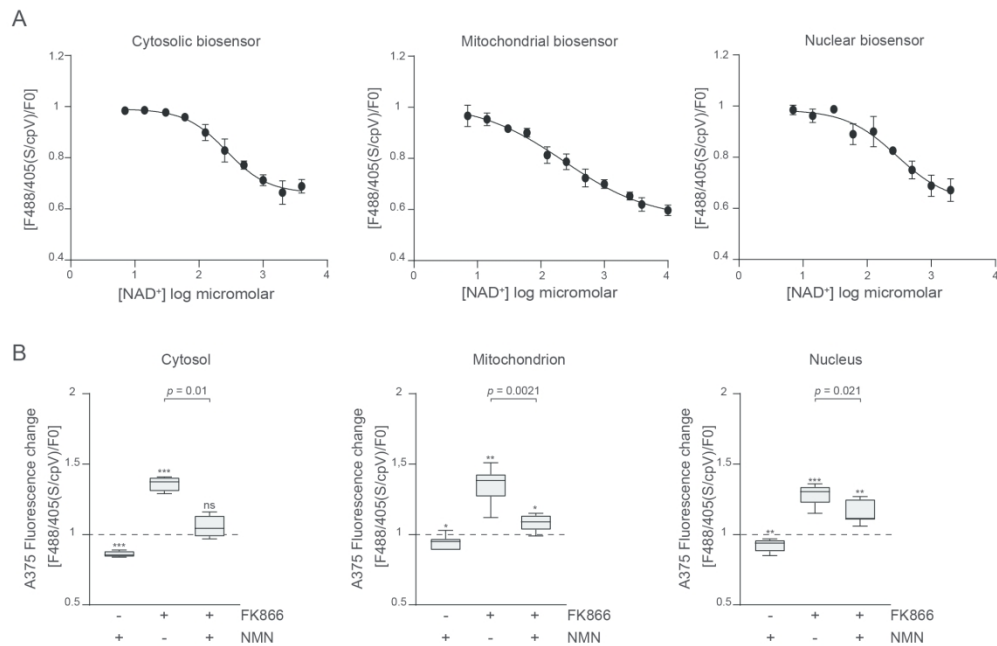


Figure 2. Effects of the NAMPT inhibitor FK866

(A) Upper: quantification of time lapse imaging of A375 cells expressing the cytosolic, mitochondrial and nuclear biosensor, in response to FK866 (25nM, 4h period). Cells were cultured on Ibidi chambered coverslips and kept at 5% CO<sub>2</sub> and 37°C during the experiment. Curves show the fluorescence ratio between 488 nm and 405 nm of the biosensor reported as a function of time. 488 nm and 405 nm fluorescence were separately recorded and the ratio was obtained by image calculator plugin of ImageJ software analysis. Curves are the results of 4 independent measurements. Lower: representative frames of A375 expressing relative biosensors at time (t) = 0 and t = 4. Fluorescence was acquired by confocal microscopy, using an oil immersion 63x objective, in the figure A cropped images from zoomed acquisition fields are shown. NAD<sup>+</sup> depletion can be followed by observing the increase of fluorescence intensity (movies 1-2-3). (B) NAD<sup>+</sup> variations measured in A375 cytosol (C), mitochondria (M) and nuclei (N) after treatment with FK866 (25 nM, 16 hours). Box plots are the results of 9 different experiments. Results are expressed as a "Ratio of Ratio" [F488/405(S/cpV)/F0]. Sensor/cpVenus (488 nm/405 nm) fluorescence ratios were measured by flow cytometry and the fold change compared with untreated controls (F0). (C) Representative example of fluorescence variation of the cytosolic biosensor upon FK866 treatment in A375.

Dot plot (on the left) and histogram (on the right) show the specificity of the NAMPT inhibitor -induced NAD<sup>+</sup> depletion in increasing biosensor 488 nm fluorescence. UN: untreated.





**Figure 3. Subcellular NAD<sup>+</sup> concentrations and effects of NMN on subcellular NAD<sup>+</sup> levels**  
(A) Calibration curve of cytosolic, mitochondrial and nuclear biosensors obtained in A375. Cells were permeabilized with 0,005% saponin (cytosolic and nuclear biosensors) or with saponin and Alamethicin (mitochondrial biosensor expressing A375) and exposed to increased exogenous concentrations of NAD<sup>+</sup>. The fluorescence ratios (488 nm/405 nm) of the biosensor were normalized to cpVENUS. Diagrams show normalized fluorescence ratios (y-axis) reported as a function of logarithmic NAD<sup>+</sup> concentrations (x-axis) and fit with a variable slope model. Curves are the results of 4 independent experiments.(B) Intracellular NAD<sup>+</sup> variations in A375 after treatment with NMN (0.5 mM, 16 hours), in presence or absence of FK866 25 nM (n=5). Results are expressed as a “Ratio of Ratio”  $[F488/405(S/coV)]/F0$ . Sensor/cpVenus (488 nm/405 nm) fluorescence ratios were measured by flow cytometry and the fold change was compared to untreated controls (F0). Two-sided paired Student’s t test was used to determine statistical significance. Star marks refer to the significance of the relative change of each treatments condition compared to the untreated (untreated=1), while the p value refers to the rescue of supplementations from the FK866-treated condition. Boxes represent interquartile range, and the horizontal line across each box indicates the median. ns= not statistically significant.

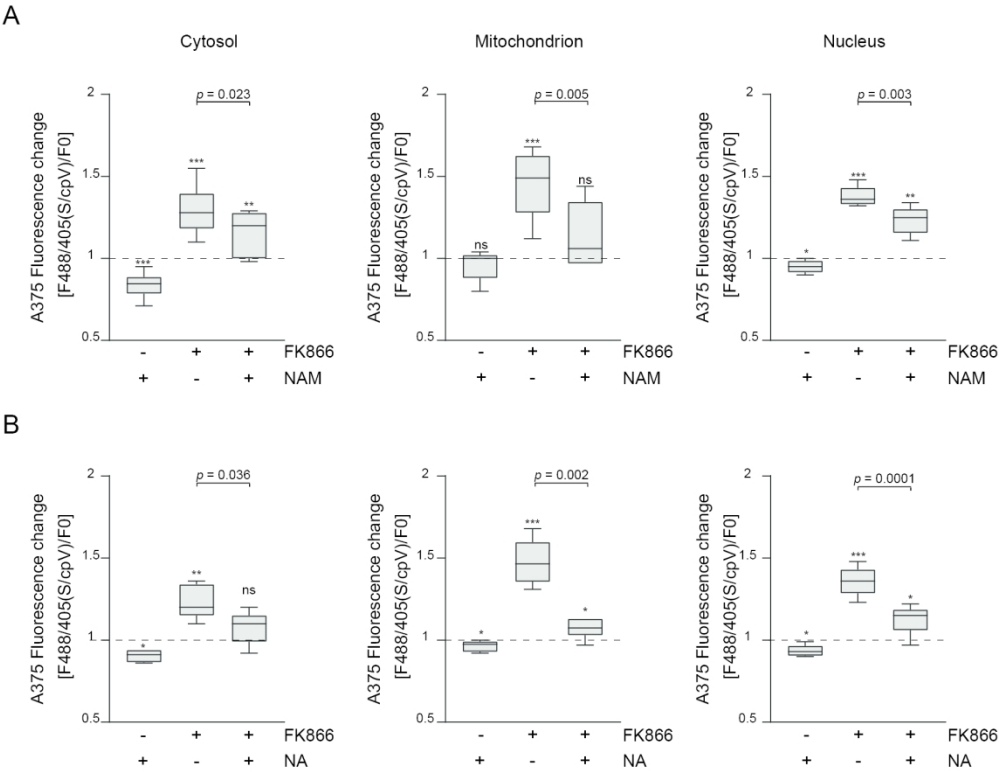


Figure 4. Topography of NAD+ Biosynthesis: NAM and NA primarily affect cytosolic NAD+ levels  
Cells were treated as follows: (A) 500  $\mu$ M NAM  $\pm$  25 nM FK866; (B) 6  $\mu$ M NA  $\pm$  25 nM FK866. Results are expressed as a "Ratio of Ratio" [F488/405(S/coV)/F0]. Sensor/cpVenus (488 nm/405 nm) fluorescence ratios were measured by flow cytometry and the fold change was compared to untreated controls (F0) (n=5). Star marks refer to the significance of the relative change of each treatments condition compared to the untreated (untreated=1), while the p value refers to the rescue of supplementations from the FK866-treated condition.

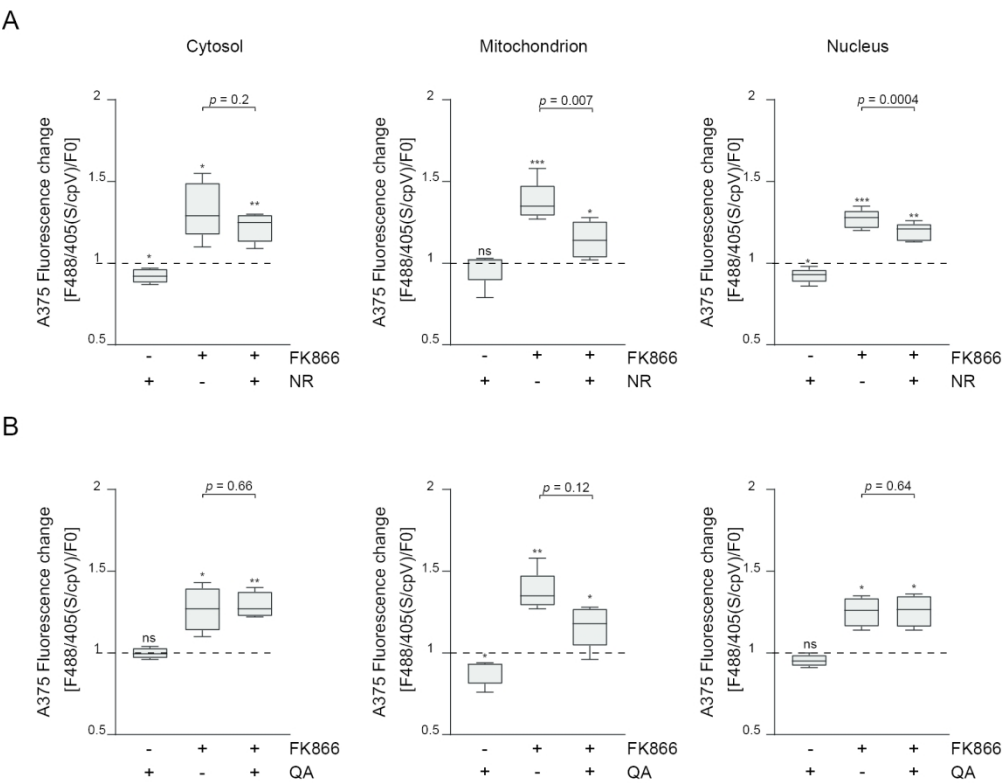


Figure 5. Topography of NAD+ Biosynthesis: NR and QA showed an organelle-specific impact on NAD+ levels

Cells were treated with (C) 100  $\mu$ M NR  $\pm$  25 nM FK866; (D) 200  $\mu$ M QA  $\pm$  25 nM FK866. A375 cells were exposed to the treatments for 16 hours. Results are expressed as a "Ratio of Ratio" [F488/405(S/coV)/F0]. Sensor/cpVenus (488 nm/405 nm) fluorescence ratios were measured by flow cytometry and the fold change was compared to untreated controls (F0) (n=5). Star marks refer to the significance of the relative change of each treatments condition compared to the untreated (untreated=1), while the p value refers to the rescue of supplementations from the FK866-treated condition.

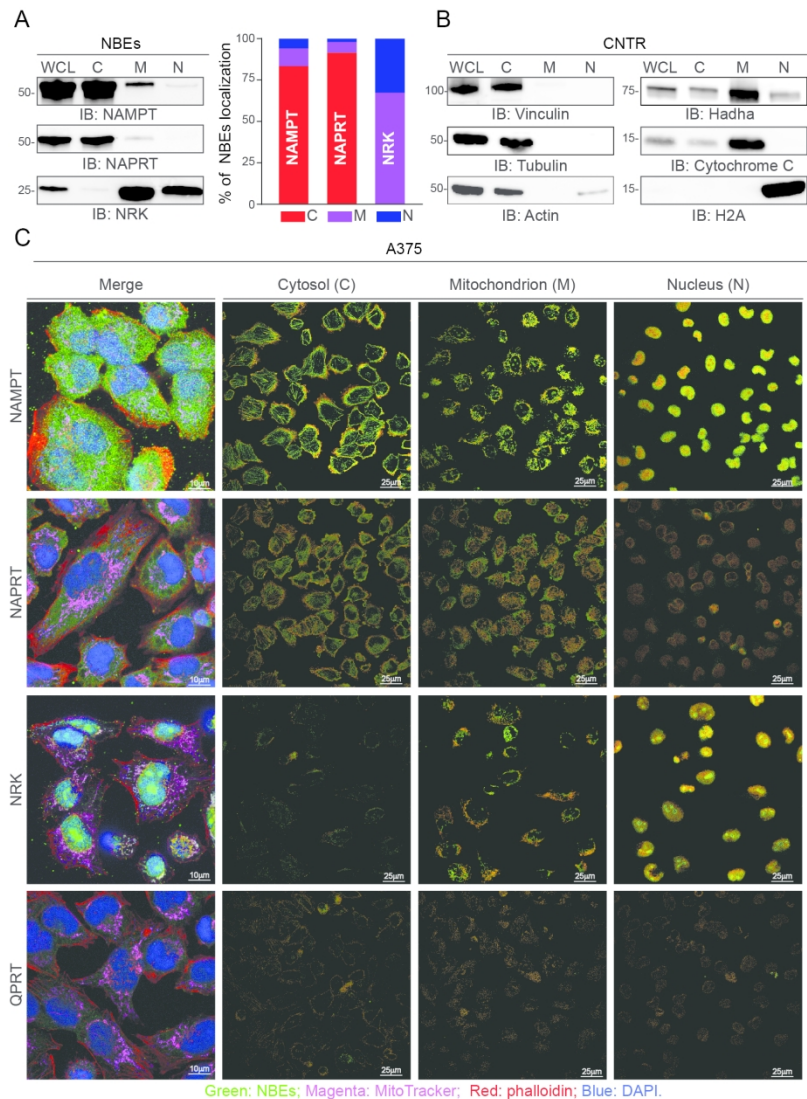


Figure 6. Subcellular localization of NAD<sup>+</sup> biosynthetic enzymes

(A) Mitochondria and nuclei were isolated as described in material and methods. 10µg of each lysate were loaded in the following order: whole cell lysate (WCL), cytosolic fraction (C), mitochondrial fraction (M) and nuclear fraction (N). Anti-Vinculin, anti-tubulin, anti-actin, anti-Hadha, anti-cytochrome c and anti-H2A were used to determine the purity of cytosolic, mitochondrial and nuclear fractions, respectively. (B) Graph represents the percentage of NBEs expression in each fraction. Band quantification was performed using ImageQuant software. Values are referred to the mean of 6 independent experiments. % was calculated as: % of pixel intensity of district specific band/sum of all districts pixel intensities. (C) On the left confocal microscopy showing NAMPT, NAPRT, NRK, QPRT total expression (green fluorescence) in whole cells (merge). Cytosol, mitochondria and nuclei were counterstained with phalloidin (red), MitoTracker (magenta) and DAPI (blue) respectively (zoomed image of 63X magnification, scale bar= 10µm). On the right NBEs-cytosol/mitochondria/nuclei sub-localization. In detail, NAMPT, NAPRT, NRK and QPRT (green fluorescence) were localized by delimiting fractions (red fluorescence) separately by using the co-localization tool of LAS AF Version Lite 2.4 software. Representative images show single NBE and single compartment overlapping

1  
2  
3  
4  
5  
6  
7  
8  
9  
10  
11  
12  
13  
14  
15  
16  
17  
18  
19  
20  
21  
22  
23  
24  
25  
26  
27  
28  
29  
30  
31  
32  
33  
34  
35  
36  
37  
38  
39  
40  
41  
42  
43  
44  
45  
46  
47  
48  
49  
50  
51  
52  
53  
54  
55  
56  
57  
58  
59  
60

(image of 63X magnification, scale bar= 25µm).

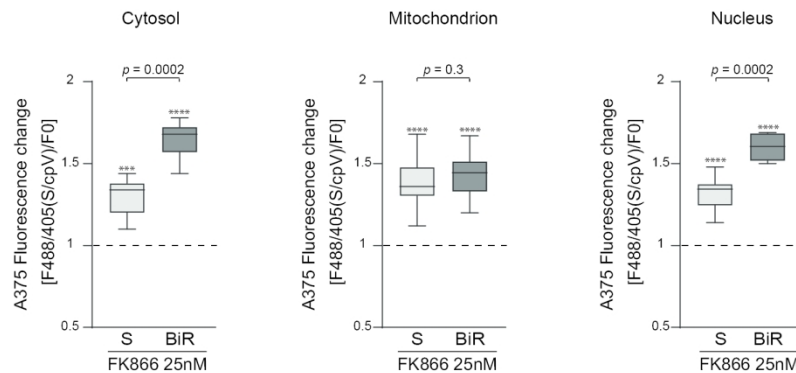


Figure 7. A375/S and /BiR responses to the NAMPT inhibition

Cytosolic, mitochondrial and nuclear NAD<sup>+</sup> variations were measured in BRAFi-sensitive (S) or resistant (BiR) cells after treatment with FK866 (25 nM, 16 hours). Results are expressed as relative fold change [F488/405(S/coV)/F0]. Sensor/cpVenus (488 nm/405 nm) fluorescence ratios were measured by flow cytometry and the fold change was compared to untreated (F0). Box plot representing 9 independent experiments. Star marks refers to the relative change of FK866 treatment compared to 1 (untreated), while p value indicates significance of the FK866 differential response of A375/BiR compared to A375/S.

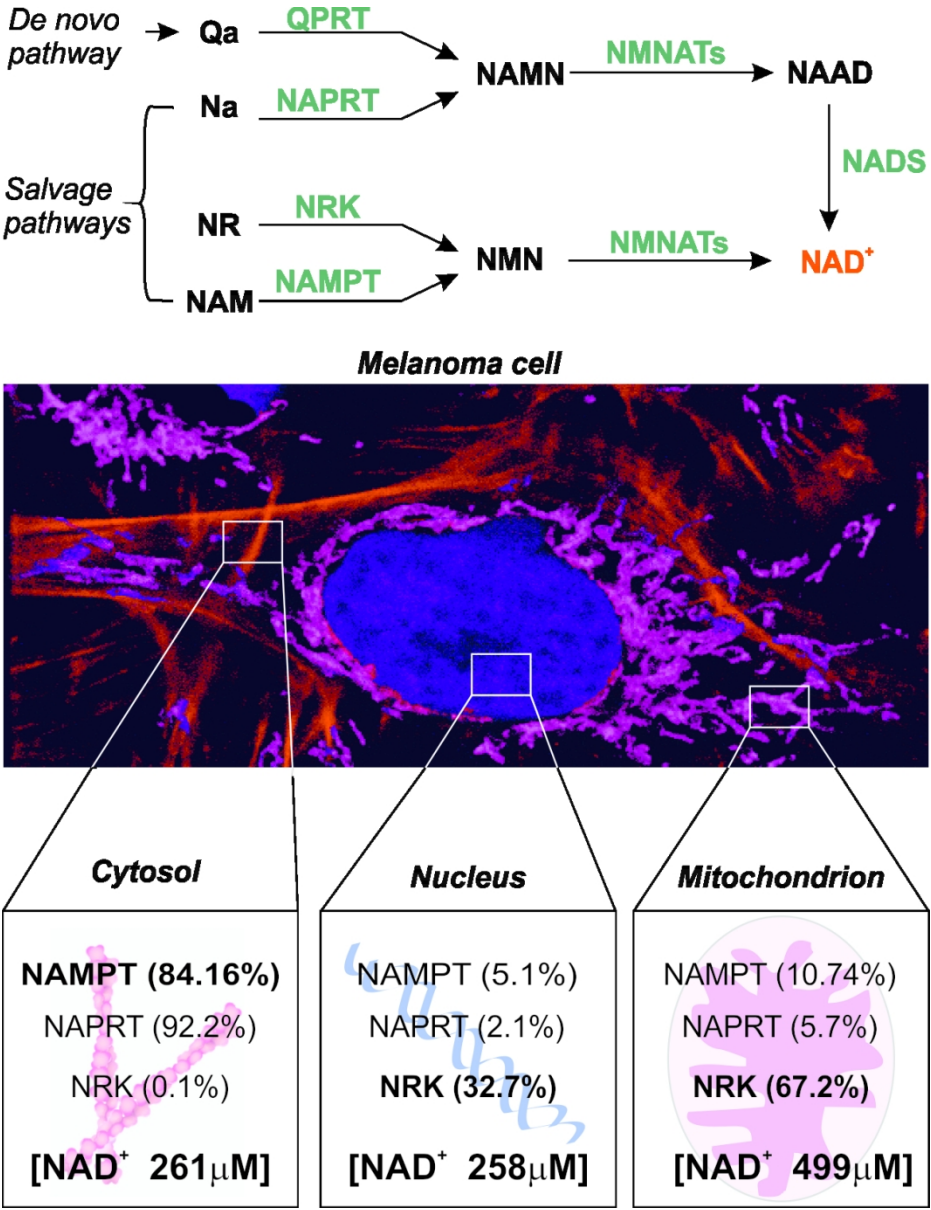


Figure 8. Compartmentalization of NAD<sup>+</sup> biosynthesis in A375 MM

On the top schematic representation of biochemical reactions involved in NAD<sup>+</sup> production. NAD<sup>+</sup> precursors present in the extracellular space can enter the cell becoming substrates of the NBEs. QA enters in the de novo biosynthetic pathway, while NA, NR and NAM are substrates of the parallel three salvage pathways. Among the NAD<sup>+</sup> precursors NAM is also the by-product of NAD<sup>+</sup> consuming enzymes such as sirtuins and PARPs. NAM and NR can be used to produce NMN by NAMPT and NRKs, respectively. NMN and NaMN (produced by NAPRT-mediated Na conversion) are finally used by compartmentalized NMNATs to generate NAD<sup>+</sup>. In the center, an A375 melanoma cell acquired by using confocal microscope. Cytosol, mitochondria and nuclei were counterstained with phalloidin (red), MitoTracker (magenta) and DAPI (blue) respectively (zoomed image of 63X magnification acquired by confocal microscopy, a cropped image is shown). Insets of A375 cytosol, nucleus and mitochondria resume the most relevant NBEs found in each A375 subcellular districts. Enzymes written in bold are the most expressed NBEs in the highlighted cell districts, while percentage refers to the expression level of each enzymes in each compartment. The cytosolic picture of A375 NAD<sup>+</sup> biosynthesis is composed by a dominant cytosolic NAMPT pathway

1  
2  
3 converting NAM into NMN. NAPRT can be considered a second, but highly active, enzyme which mediates the  
4 cytosolic NA conversion to NaMN, indeed its localization was found to be more than 92% cytosolic. These  
5 pathways contribute to the generation of an NAD<sup>+</sup> pool calculated to be around 261  $\mu$ M. In the nucleus, the  
6 NAD<sup>+</sup> pool is approximately 258  $\mu$ M and the primary expressed NBEs is NRK. In this compartment, we were  
7 also able to detect low levels of NAMPT and NAPRT (5.1% and 2% of their total expression, respectively).  
8 NRK expression is also prevalent in mitochondria (67.2 % of its total biochemical detection), where the  
9 calculated NAD<sup>+</sup> concentration is 499  $\mu$ M. In this organelle, low expression of NAMPT (10.74%) and NAPRT  
10 (5.7%) could contribute to the maintenance of mitochondrial NAD<sup>+</sup> pool.  
11  
12  
13  
14  
15  
16  
17  
18  
19  
20  
21  
22  
23  
24  
25  
26  
27  
28  
29  
30  
31  
32  
33  
34  
35  
36  
37  
38  
39  
40  
41  
42  
43  
44  
45  
46  
47  
48  
49  
50  
51  
52  
53  
54  
55  
56  
57  
58  
59  
60

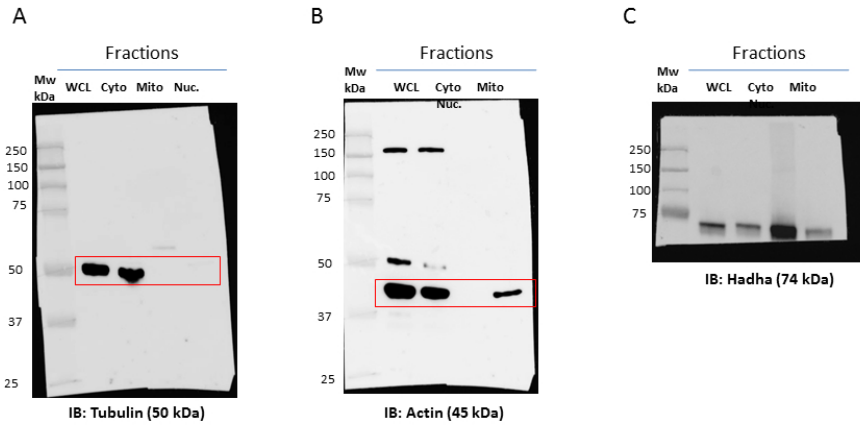


Table 1

[NAD <sup>+</sup> μM]	Cytoplasmic F488/F405 (S/cpV)	Mitochondrial F488/F405 (S/cpV)	Nuclear F488/F405 (S/cpV)
0	1	1	1
0.7	0.988	0.98	0.995
15	0.986	0.953	0.973
30	0.98	0.92	0.988
60	0.954	0.9	0.9
125	0.899	0.813	0.91
250	0.838	0.78	0.84
500	0.776	0.723	0.76
1000	0.71	0.7	0.712
2000	0.668	0.653	0.68
4000	0.66	0.62	N.D.
10000	N.D.	0.596	N.D.

Table 1. Fluorescence variations of each biosensors in the presence of NAD+  
Table showing cpVENUS normalized fluorescence variations of each biosensors when exposed to increasing concentrations of exogenous NAD+ in a condition of saponin or saponin/alamethicin-mediated permeabilization. Reported numbers are the mean of four independent experiments for cytosolic and nuclear biosensor, of three independent experiments for mitochondrial biosensor.

WCL = whole cell lysates  
Cyto = cytoplasmic lysates  
Mito = mitochondrial lysate  
Nuc = nuclear lysates  
Mw = Molecular weight



Full unedited of western blot analysis: Figure 6.

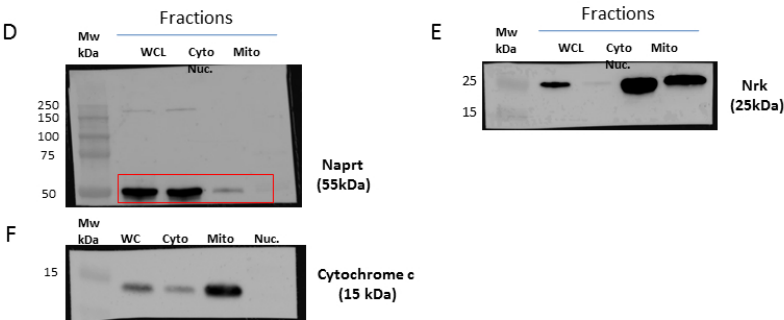
A-B: anti-tubulin and anti-actin used as loading controls of cytoplasmic fractions → Figure 6B of the manuscript, second and third cropped western blot on the left.

C: anti-Hadha used as mitochondrial marker → Figure 6B of the manuscript, first cropped western blot on the right.

254x190mm (96 x 96 DPI)

1  
2  
3  
4  
5  
6  
7  
8  
9  
10  
11  
12  
13  
14  
15  
16  
17  
18  
19  
20  
21  
22  
23  
24  
25  
26  
27  
28  
29  
30  
31  
32  
33  
34  
35  
36  
37  
38  
39  
40  
41  
42  
43  
44  
45  
46  
47  
48  
49  
50  
51  
52  
53  
54  
55  
56

WCL = whole cell lysates  
Cyto = cytoplasmic lysates  
Mito = mitochondrial lysate  
Nuc = nuclear lysates  
Mw = Molecular weight



Full unedited of western blot analysis: Figure 6.

D-E: anti-Naprt and anti-NRK used for NBEs detection in the different subcellular fractions → Figure 6A of the manuscript, second and third cropped western blot.

F: anti-Cytochrome c used as mitochondrial marker → Figure 6B of the manuscript, second cropped western blot on the right.

254x190mm (96 x 96 DPI)

1  
2  
3  
4  
5  
6  
7  
8  
9  
10  
11  
12  
13  
14  
15  
16  
17  
18  
19  
20  
21  
22  
23  
24  
25  
26  
27  
28  
29  
30  
31  
32  
33  
34  
35  
36  
37  
38  
39  
40  
41  
42  
43  
44  
45  
46  
47  
48  
49  
50  
51  
52  
53  
54  
55  
56  
57  
58  
59  
60